Georgia Tech Sponsored Research

Project	E-20-F09 S2656
Project director	Santamarina Juan
Research unit	CEE
Title	Joint Studies Between Intevep and Georgia TechJoint Studies Between Intevep and Georgia
Project date	12/31/1999

66

E-20-F09

Georgia Institute of Technology

Dept. of Civil and Environmental Eng.

TOMOGRAPHY OF THE STATE OF STRESS

LAGUNILLAS FIELD TEST

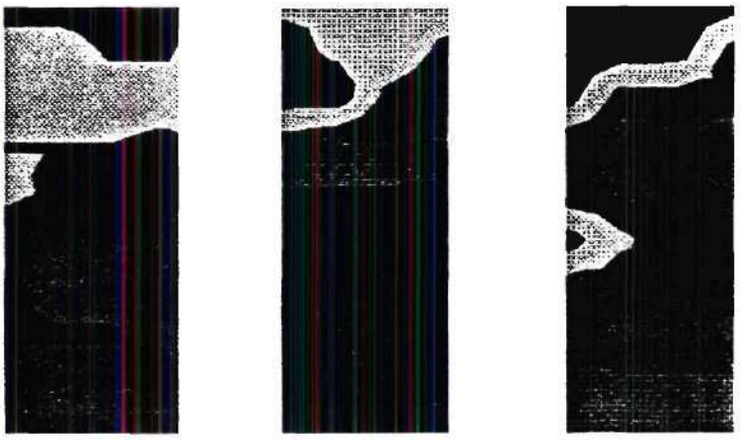

Prepared by

J.C. Santamarina and A.L. Fernandez

January 2000

TOMOGRAPHY OF THE STATE OF STRESS

LAGUNILLAS FIELD TEST

1. Introduction

The purpose of the field test is to implement the wave-based characterization of a site using the tomographic techniques described previously, and to assess the applicability of this methodology as a conventional testing method in view of engineering needs. Improvements in hardware are also introduced in order to increase the quality of the measurements. Such improvements focus on the testing of the new "borehole-less" source of shear-waves.

The fieldwork includes three crosshole tests performed in the same soil deposit, but under different states of stress. Ultimately, the solution is interpreted in terms of the state of stress. Additional data from prior complementary studies are included.

2. Site Description

Tomographic imaging of the state of stress is enhanced when, a given soil deposit is tested under different states of stress. Three tests in Lagunillas, Venezuela, are performed at one of the dams within the Lake Maracaibo Coastal Protection System. This site is selected because:

1. It is a region of major subsidence and critical for the safety of the population and onshore facilities.
2. It gives the opportunity to test the same deposit of soil under three different states of stress.
3. The soil profile is well characterized.
4. Support facilities (water, electricity, accessibility, restricted traffic and availability of human resources) are readily available.
5. The site was previously tested with complementary techniques on July 1996.

The first test (Natural Field Test, NFT) is executed approximately 7.0m downstream from the toe of the dam, away from the area of influence of the dam. The second test (Berm Test, BRT) is executed on a stabilization berm on the downstream shoulder of the dam, at a distance of 28.0m from the NFT. At this location, the berm is about 2.8m high, which represents an overburden pressure of 56 kPa. Finally, the last test (Top of the Dam Test, TDT) is executed on the crest of the dam, separated 49.0m from the BRT and 77.0m from the NFT. The relative elevation of this site is approximately 7.2m over the ground surface (NFT). The overburden pressure at this location due to the weight of the dam is about 145 kPa (Fig. 1).

3. Soil Profile

The soil deposit in this area consists of two well differentiated materials. The near surface layer is a non-plastic silt (ML), with soft to medium consistency. This layer is about 4.5m thick, and appears to be normally consolidated. The shear-wave velocity distribution and the SPT profile increase with depth.

The second layer consists of a high plasticity clay with very soft consistency. The thickness of this layer is at least 6.0 m. SPT data show a blow count lower than or equal to 1 along the whole layer. It is also noticed that, the water content is near the liquid limit, and sometimes above, which suggests light sensitivity (Fig. 2).

4. Test Setup

The experimental design is based on a regular crosshole test setup, but with the following relevant differences: (1) there is only one cemented-cased borehole where the array of receivers is placed. (2) The source is driven into the soil with a CPT equipment. (3) Hydrophones are used instead of regular well geophones, which implies that the borehole is kept filled with water during the test (hydrophones do not need to be oriented, they have good coupling with the casing, and they can be placed or removed fast and easily). (4) The signal generated is recorded at all the receivers instead of just the horizontal receiver (Fig. 3).

The source is driven 3.0m away from the borehole that contains the receivers, and the measurements are taken every meter. Receivers in the hydrophone array are placed every 1.0m as well. The geometric details for each test appear in Table 1 an in Fig. 4

The acquisition system consists of a 12-channel Bison seismograph (Model 5000) connected directly to the hydrophones and triggered by an inertial transducer placed inside the source. The acquired signals are stacked 16 or 32 times and stored in a PC. The sampling rate interval is set at $\Delta t = 0.025$ msec for a record length of 75.0 msec. The signals are also filtered using a built-in band-pass filter: 8.0 Hz high-pass and a 2.0 kHz low-pass.

5. Prior Characterization of the Berm

Previous studies have been performed to characterize the berm using surface techniques without boreholes (1996 field tests). They include seismic reflection/refraction tests done in the normal and parallel directions with respect to the main axis of the dam (Fig. 5).

The arrival of surface Raleigh-wave can be clearly distinguished. Given the multiplicity of sources and receivers, reliable parameters for the berm can be

determined. The computed R-wave velocity is significantly higher than velocities measured for uncompacted materials at similar stress levels. This indicates the stabilizing effect of compaction, the effects of residual horizontal stresses within the medium and the increased effective stress due to partial saturation (Figs. 6 and 7).

Wave velocities are used to compute the azimuthal anisotropy in the state of stress on the horizontal plane. The ratio between R-wave velocities in the directions parallel and normal to the dam indicates a stress ratio on the horizontal plane of approximately 2.3, where the state of stress is greater in the direction normal to the axis of the dam which normal to the direction of compaction. An alternative or concurrent mechanism effect is the bending and stretching of the dam as a beam in the axial direction, in response to the ongoing subsidence of the subsurface, and the corresponding reduction in effective stress.

6. Signal preprocessing based on P-wave Data

Preprocessing the data gives an additional insight about the field test, and how the data were gathered (e.g. information content and background noise level). It also shows general trends about the area under study, such as the presence of anomalies and anisotropy. This additional information can be used to improve the tomographic inversion (e.g. initial guess, weighted measurements, and regularization). In addition, it helps in the identification of possible measurement errors and in the selection of corrective measures.

P-waves can be used to detect certain errors, such as geometry and triggering errors. The underlying assumption is that the P-wave velocity in quasi-saturated soils is little sensitive to soil conditions (such as skeleton stiffness or anisotropy). Possible diagnostic observations can be gathered from the following logic:

- If all signals for a single shot are used to plot travel time vs. distance and a non-zero time intercept is observed, then trigger delay error should be expected.
- If the computed velocities are greater than the values that can be justified for a saturated medium, then the geometry of the array must be corrected to compensate for this error (in this case, the distance between sources and receivers should be increased).

- If the computed velocities are lower than the values corresponding to a saturated medium, either the assumed relative position between sources and receivers is greater than the real value, or the medium is not fully saturated. To solve this non-uniqueness, additional information should be provided, such as inclinometer data to verify the position of the transducers, or saturation parameters for the soil should be obtained.

P-wave velocity shadows for the Lagunillas study show an increase in the velocity with shooting angle. However, in this case, anisotropy can be discarded because this phenomenon only appears for the rays shooting upwards (and V_p is mostly isotropic in saturated soft sediments). It is hypothesized that the wave transmitted along the rods above the source radiate enough energy to cause the early arrivals. To test this possible explanation, velocity shadows are plotted again, but assuming that the measured travel time is spent in horizontal travel, in all upwards shots. The resulting shadows lock the initial observed anisotropy. That means that, for the upward shots, the waves are being transmitted through the rods. It is concluded that the average P-wave velocity in the three studies varies between V_p= 775 m/s and V_p = 1050 m/s (Fig. 8).

As for trigger or geometry effects, there is no conclusive evidence that show a significant effect in any case. The only remarkable observation that can be made

is when there is a "jump" between velocity shadows (like the one on the last plot of Fig. 8.b), in this case, the possible cause is a trigger error responsible for the jump in velocity.

The P-wave velocity is highly sensitive to the degree of saturation of the medium. Mathgram 1 shows the computation of the P-wave velocity as a function of the saturation, S and the porosity, n. It can be inferred that, for the mean P-wave velocity observed in Mathgram 1, the value of saturation ranges from S = 0.9996 to S = 0.9999 depending on the porosity of the soil. This determination of the degree of saturation is very convenient to assess the liquefaction potential of a geomaterial. Related charts by Ishihara (1998) and Head (1986), shown in Fig. 9, can be used to determine Skempton's B. From Ishihara's data and for V_p<1000m/s, B<0.95. According to Head's Chart, Skempton's B parameter is around B = 0.9998.

The main conclusions from P-wave data preprocessing are:

- Energy is being transmitted and radiated along the rods above the source.
- No significant trigger error or crosshole geometry deviation can be detected.
- The medium is not fully saturated. A Skempton's B value is expected to be between B<0.95 to B ≈ 0.9998. This can improve the liquefaction resistance.

7. Shear Wave Data

Typical traces are shown in Fig. 10 where the apparent shear-wave front is indicated. Computed horizontal shear-wave velocity profiles for the three tests are consistent with the soil profile defined by SPT data, showing the existence of the normally consolidated material lying over the very soft deposit (Fig. 11, only horizontal rays are included). It is observed in this plot, that the overburden stress contributed by the dam has a significant effect on the upper layer, while its effect on the lower layer cannot be readily appreciated.

7.1 Preprocessing - S-wave velocity shadows

Before attempting to invert the travel time data to obtain tomographic images of the subsurface, data preprocessing is implemented to get a preliminary understanding of the test performance and of the geomedium, including stratigraphy and the potential presence of anomalies.

The velocity shadows appear to be smooth without any relevant localized peak (Fig. 12 and 13). The presence of peaks in the shadows might be an indication that there is an anomaly buried in the deposit.

The plot of shear wave velocity against ray inclination suggests strong anisotropy in the computed average velocities: the shear-wave velocity increases as the shooting angle increases, up to 2.5 times for the maximum shooting angle of 70 degrees. It is not possible to justify anisotropy greater than 1.1 to 1.25 in normally consolidated soils. One hypothesis that is considered to explain these results involves horizontal travel at the average S-wave velocity V_s, plus travel along the casing with tube-wave velocity V_{tube}. This analysis renders travel times comparable to the measured times when V_{tube} = 550 m/s for the three locations (Fig. 14). Such tube-wave velocity can be analytically supported for the test conditions, as shown in Mathgram 2.

With this information, the reverse analysis is implemented to select "credible shots" by identifying the corresponding arriving events in the traces: both the direct and the soil-tube arrival (Fig.15). Only those shots where the direct arrival is not masked by the tube-wave are considered "credible", and used for tomographic imaging. It is observed that credible shots are restricted to limited illumination angles.

8. Tomography

Once first arrivals are identified, the tomographic images are generated using all horizontal rays plus other rays with credible S-arrival detection. This selection criterion reduces the number of ray to those with a shooting angle smaller the 40 degrees. Given that these rays are at low inclination, the resulting, tomographic images should be considered "narrow beam" based.

Two sets of tomographic images are presented. Both sets use the regularized least square solution. The first inversion uses a regularization matrix based on the 2D-smoothing kernel:

$$\text{Regularization kernel for global smoothness} = \begin{bmatrix} 0 & 1 & 0 \\ 1 & -4 & 1 \\ 0 & 1 & 0 \end{bmatrix}$$

The boundary pixels are smoothed using the reflective criterion. The tomographic images obtained with this type of inversion are shown in Fig. 16. The optimal value of λ was selected as 300 (see Fig. 17 for the effect of λ on error and inverted min and max velocities).

For the second set of images, the development of a regularization matrix based on a horizontal smoothing kernel recognizes the predominately horizontal layered stratigraphy:

$$\text{Horizontal smoothing kernel} = \begin{bmatrix} 1 & 1 & 1 \\ 3 & 3 & 3 \\ 1 & 1 & 1 \end{bmatrix}$$

It is important to mention that in this case that the criterion to be minimized captured in the regularization matrix is the distance between the horizontally smoothed value and the original value (Santamarina & Fratta, 1998), rendering a:

$$\text{Regularization kernel for horizontal smoothness} = \begin{bmatrix} 1 & 1 & 1 \\ 3 & -12 & 3 \\ 1 & 1 & 1 \end{bmatrix}$$

In this case the boundary kernels assume "non-reflective" boundaries. The tomographic images obtained with this inversion are shown on Fig. 18. The optimal value of λ was selected as 300

9. Engineering Implications

The following analysis is conducted to correlate the shear-wave measurements with the theoretical values. The analysis consists of 3 stages:

1. Pore pressure estimation: A simple flownet is drawn under the body of the dam, and the piezometric pressure at the location of each test is computed using the method of fragments (Fig. 19).
2. Estimation of vertical effective stress: the effective stress is computed as the difference between the total overburden pressure (produced by the overlaying strata and the body of the dam) and the pore water pressure computed from the flownet.
3. Estimation of the shear wave velocity based on the relationship:

$$Vs = \alpha \cdot \left[\frac{\sigma'_v}{(1 \cdot kPa)} \cdot \frac{(1 + k_o)}{2} \right]^{\beta}$$

where the values of α and β are obtained from the measured data (based on initial values from laboratory study by Santamarina et al.1995).

The value of α is defined as the value of V_s for 1.0 kPa mean applied stress on the polarization plane. A compilation of α and β values is presented on Table 2 and in Fig. 20. It is observed that α and β values are related: the softer and more clayey the soil is, the lower the value of α and the higher the value of β. The following correlation is appropriate:

$$\beta = 0.35 - \frac{\alpha(m/s)}{800}$$

The estimated values of the S-wave velocity are plotted in Fig. 21 and 22 along with the horizontal shot measurements previously presented on Fig. 11.

Two prediction lines are shown. The one in Fig. 21 is based on α and β values used to fit the NFT data (satisfying $\beta = 0.35 - \alpha/800$). From this fit, it is concluded that the state of stress under the berm is lower than expected (the berm may be arching, recall preliminary study of Lagunillas - Section 4).

The fitting in Fig.22 correspond to the best fit using α and β values that fulfill the relationship $\beta = 0.35 - \alpha/800$ in each layer. It is concluded that it is possible to fit the measurements, however, if this is the case, there are significant differences in soil conditions between the three tomographic locations.

10. Conclusions

Several conclusions can be drawn from this field study

- Although the cone-type source appeared to perform well in the field, the cone source transmits energy along the rods, causing early arrivals in receivers above the source location. The design should be improved in such a way that the source tip is mechanically isolated from the rest of the rod system during excitation in order to avoid wave generation through the rods.
- The use of hydrophones as receivers in boreholes filled with water is inappropriate for tomographic applications, especially when the soil is very soft and the soil/case impedance increases and/or when the tube velocity is greater than the shear wave velocity in the medium. The result is a strong tube-wave component that interferes with the arrival of the shear-wave. This is probably the case in most near surface soil sites where borehole casing is used. Narrow beam tomography is strongly suggested in this case.
- Preprocessing P-wave data is a powerful tool to assess systematic errors, such as geometry setup or trigger delays. In this case it allowed to recognize the transmission an emission of the P-waves through the rod system.
- The prevailing P-wave velocity in the foundation soil is between 800 - 1000 m/s. Therefore, the subsurface is not saturated, and values of saturation range between $S = 0.9996$ and $S = 0.9999$. The corresponding Skempton's B parameter varies between $B \approx 0.95$ and $B = 0.9998$.

- The shear-wave velocity inversions show two different soil strata in the three locations. The top layer has remarkably higher velocity than the lower layer probably due to dissecation during formation.
- The shear wave velocity increases between the natural field and the top of the dam sites, probably due to the effect of the additional overburden pressure. However, the velocity below the berm is lower than in the other two locations. Soil variability and/or unexpectedly low state of stress should be considered.
- Horizontal smoothing kernels are preferred in layered stratigraphy such as lacustrian sedimentation.
- Tomography is a powerful tool to characterize a soil deposit, not only because it gives an image of the medium, but also because the preprocessing stage provides detailed insight into the material under study, enhancing the understanding of the material properties and the performance of the field test.

11. References

- Head, K.H. (1986) "Manual of Soil Laboratory Testing. Vol.3: Effective Stress Tests" *ELE International Limited*, Pentech Press.

- Ishihara, K.; Huang, Y. and Tsuchiya, H. (1988) "Liquefaction Resistance of Nearly Saturated Sand as Correlated with Longitudinal Wave Velocity" *Proceedings of the Biot Conference in Poromechanics*. Belgium. Sept, 1998, pp.583-586

- Santamarina, J.C.; Fam, M.; Fratta, D. and Cascante, G. (1995) "Standard and Wave Based Characterization of the Lagunillas-1 Specimen" *Technical Report presented to INTEVEP*, University of Waterloo.

- Santamarina, J.C. and Fratta, D. (1998) "An Introduction to Discrete Signals and Inverse Problems in Civil Engineering". *ASCE Press*.

- White, J.E., (1983), "Underground sound. Application of Seismic Waves. Methods in Geochemistry and Geophysics", vol. 18, pp. 193-230, *Elsevier* New York.

Table 1 Geometry of the tests

Test	Crosshole Separation (m)	Depth R (m)	Depth S (m)
NFT	2.67	0.25	0.50
BRT	3.06	1.70	2.04
TDT	3.00	1.83	1.60

Separation: Horizontal distance between sources and receivers
Depth R: Depth of the first receiver (absolute elevation)
Depth S: Depth of the first position of the source (absolute elevation)

Mathgram 1 : P-Wave Velocity Computation

Assumed values for Saturation, S, and Porosity, n :

$$j := 0..50 \qquad i := 0..32 \qquad S_j := 1 - \frac{j}{10000} \qquad n_i := 0.20 + \frac{i}{40}$$

Unit weights and density:

$$\gamma_s := 26.5 \cdot 10^3 \cdot \frac{newton}{m^3} \qquad \gamma_w := 10 \cdot 10^3 \cdot \frac{newton}{m^3} \qquad \rho mix_{i,j} := \left[\left(1 - n_i\right) \cdot \frac{\gamma_s}{g} + n_i \cdot \frac{\gamma_w \cdot S_j}{g} \right]$$

Shear Stiffness Parameters:

$$V_s := 120 \cdot \frac{m}{sec} \qquad G := \left(\frac{18 \cdot 10^3 \cdot \frac{newton}{m^3}}{g} \right) \cdot V_s^{\,2} \qquad G = 2.643 \cdot 10^7 \cdot Pa$$

Elastic Moduli:

$$B_w := 2.1 \cdot 10^9 \cdot Pa$$

$$B_a := 0.14 \cdot 10^6 \cdot Pa$$

$$B_s := 70 \cdot 10^9 \cdot Pa$$

Dry Bulk Modulus: $\mu := 0.1$

$$B_{dry} := \frac{2 \cdot (1 + \mu)}{3 \cdot (1 - 2 \cdot \mu)} \cdot G$$

Bulk Modulus Fluid:

$$B_{f_j} := \frac{1}{\frac{S_j}{B_w} + \frac{1 - S_j}{B_a}}$$

Bulk Modulus Mix:

$$B_{mix_{i,j}} := B_{dry} + \frac{1}{\left(\frac{1 - n_i}{B_s} + \frac{n_i}{B_{f_j}} \right)}$$

Constrained Modulus:

$$M_{i,j} := B_{mix_{i,j}} + \frac{4}{3} \cdot G$$

P-wave Velocity:

$$V_{p_{i,j}} := \sqrt{\frac{M_{i,j}}{\rho mix_{i,j}}}$$

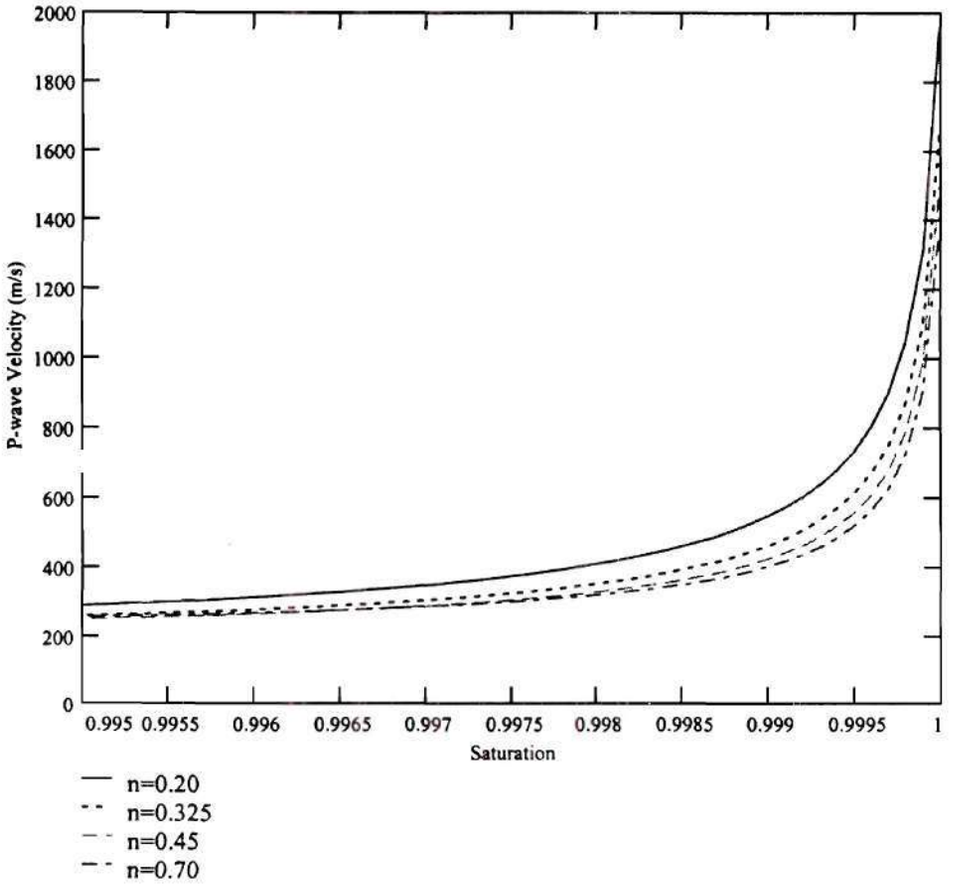
2000
1800
1600
1400
1200
1000
800
600
400
200
0
P-wave Velocity (m/s)
0.995 0.9955 0.996 0.9965 0.997 0.9975 0.998 0.9985 0.999 0.9995 1
Saturation
n=0.20
n=0.325
n=0.45
n=0.70

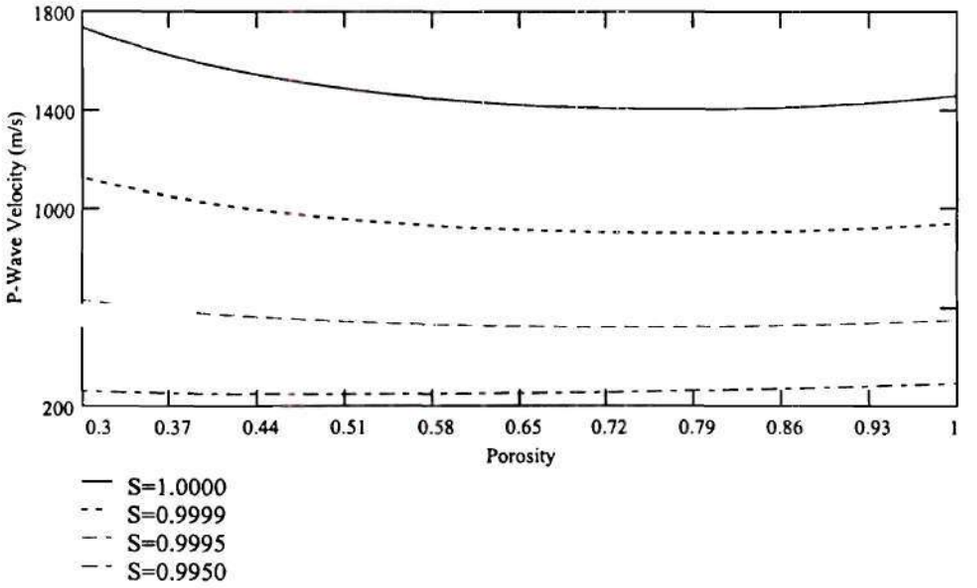
1800
1400
1000
200
P-Wave Velocity (m/s)
0.3 0.37 0.44 0.51 0.58 0.65 0.72 0.79 0.86 0.93 1
Porosity
S=1.0000
S=0.9999
S=0.9995
S=0.9950

Mathgram 2: Tube-Wave Velocity Computation

(Reference: White, J.E. (1983) "Underground Sound. Application to Seismic Waves" Elsevier

Casing Geometry: $OD := 4 \cdot in + 2 \cdot cm$ $ID := 4 \cdot in$ $t_p := \frac{OD - ID}{2}$ $t_p = 10 \cdot mm$

Young's Modulus for PVC casing: $E_{pvc} := 2 \cdot 10^9 \cdot Pa$ $a := OD$ $b = ID$

Young's Modulus for cementing slurry: $E_c := 4 \cdot 10^9 \cdot \frac{newton}{m^2}$ Nylon pipe poorly cemented

Assuming $\delta_c = \delta_{pvc}$ $F_c + F_{pvc} = T_{tot}$ $\Rightarrow \varepsilon \cdot E_c \cdot A_c + \varepsilon \cdot E_{pvc} \cdot A_{pvc} = \varepsilon \cdot E_{eq} \cdot A_{tot}$

$E_c \cdot A_c + E_{pvc} \cdot A_{pvc} = E_{eq} \cdot A_{tot}$

Poisson's ratio: $\mu := 0.15$

Equivalent Young's Modulus for cemented casing: $E_{eq} := \frac{E_c \cdot \pi \cdot (OD^2 - ID^2) + E_{pvc} \cdot \pi \cdot ID \cdot t_p}{\pi \cdot (OD^2 - ID^2) + \pi \cdot ID \cdot t_p}$ $E_{eq} = 3.629 \cdot 10^9 \cdot Pa$

Fluid Properties: Unit Weight $\gamma := 9800 \cdot \frac{newton}{m^3}$ Density $\rho := \frac{\gamma}{g}$

Elastic Moduli: $M := \frac{E_{eq} \cdot (a^2 - b^2)}{2 \cdot [(1 + \mu) \cdot (a^2 + b^2) - 2 \cdot \mu \cdot b^2]}$ $M = 3.142 \cdot 10^8 \cdot Pa$

$B := \frac{E_{eq}}{3 \cdot (1 - 2 \cdot \mu)}$ $B = 1.728 \cdot 10^9 \cdot Pa$

Tube-wave Velocity: $V_T := \left[\rho \cdot \left(\frac{1}{B} + \frac{1}{M} \right) \right]^{-\frac{1}{2}}$ $V_T = 515.813 \cdot \frac{m}{sec}$

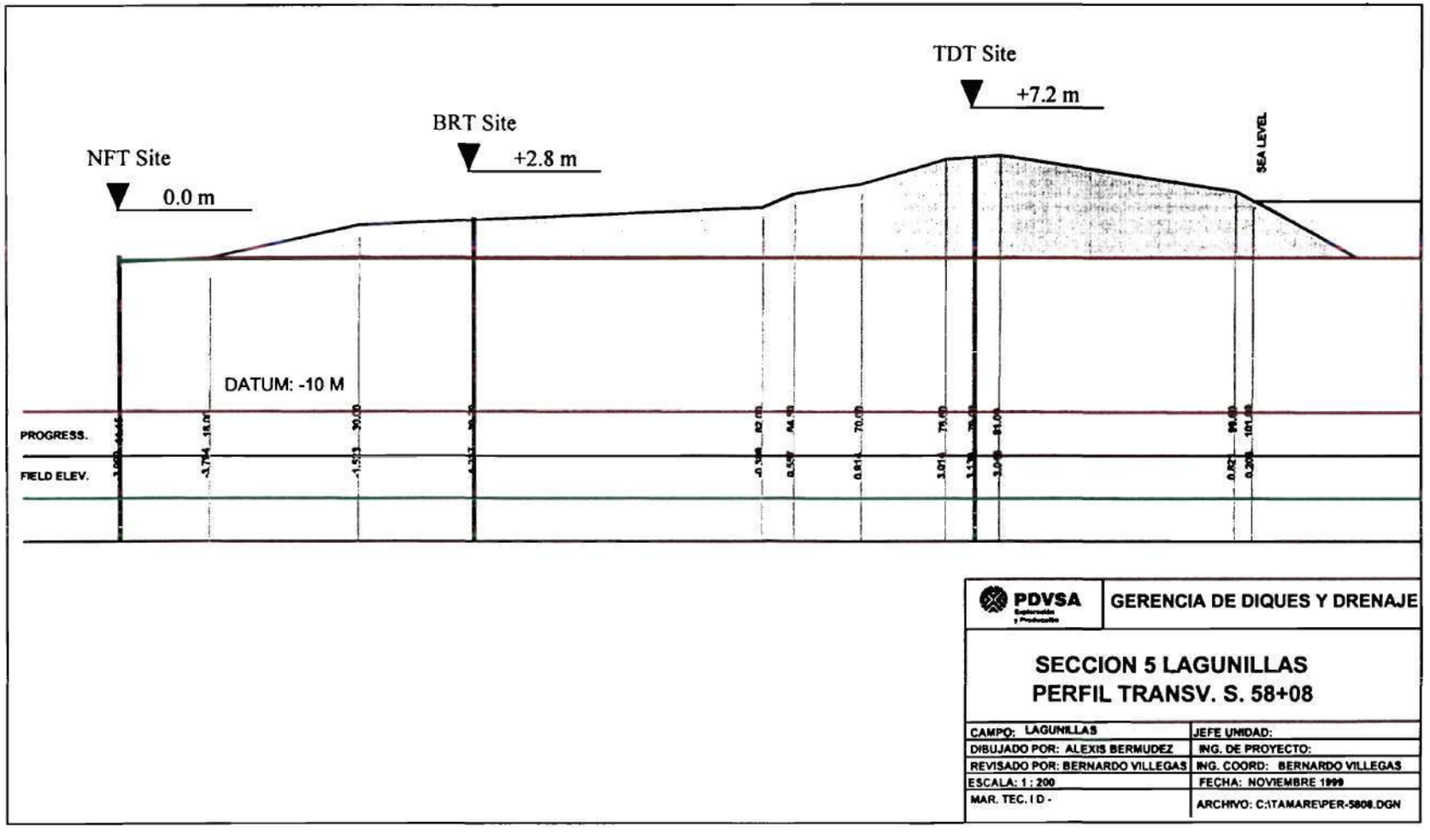

Fig. 1 Cross section of the test site - Lagunillas

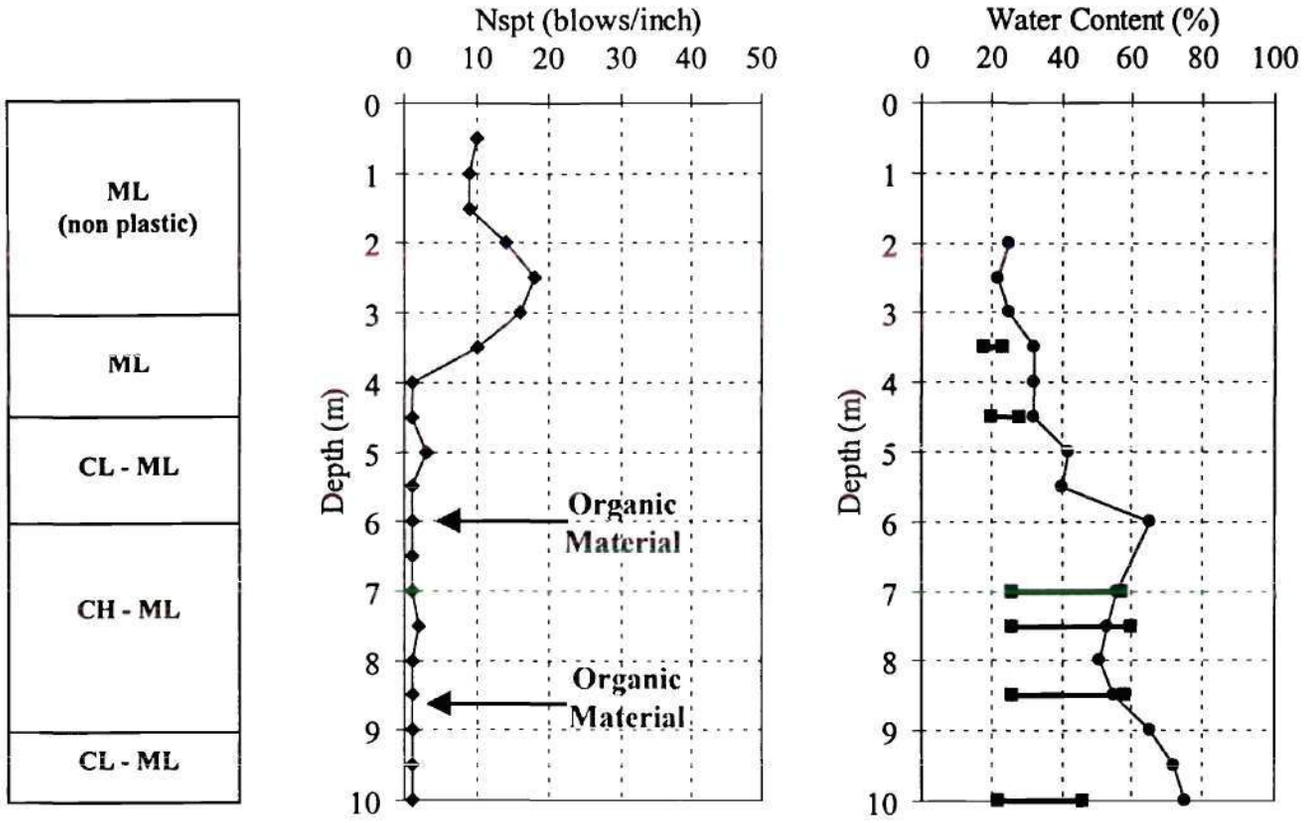

Fig. 2 SPT test - Test Site [1990 campaign]

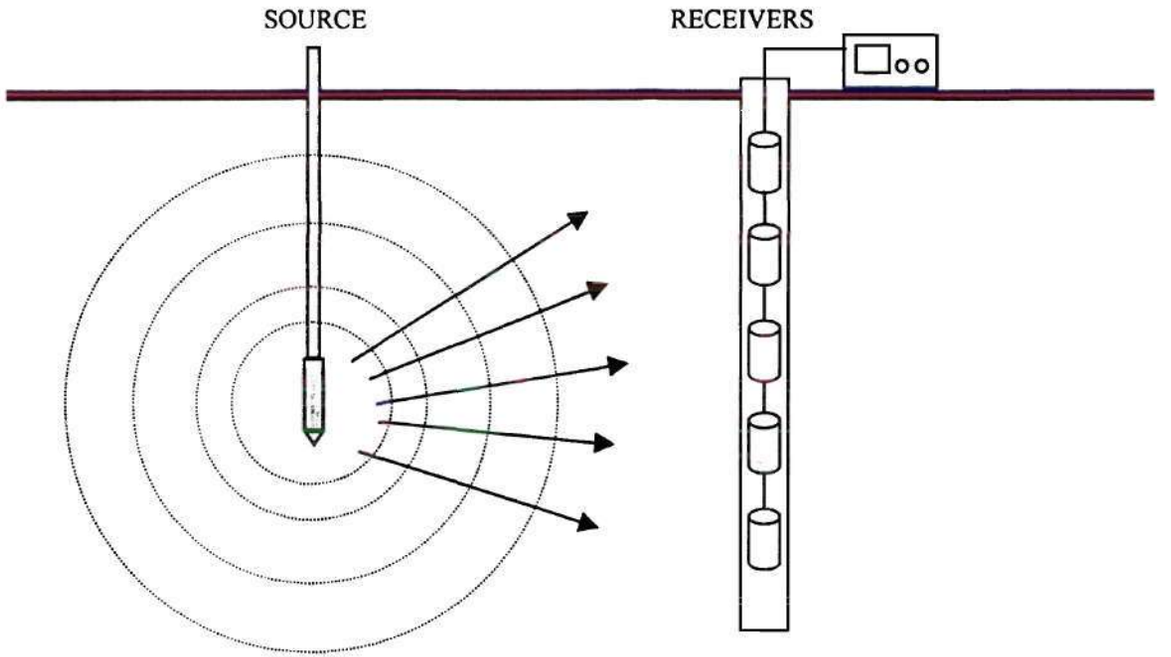

Fig. 3 Sketch of the Field Implementation

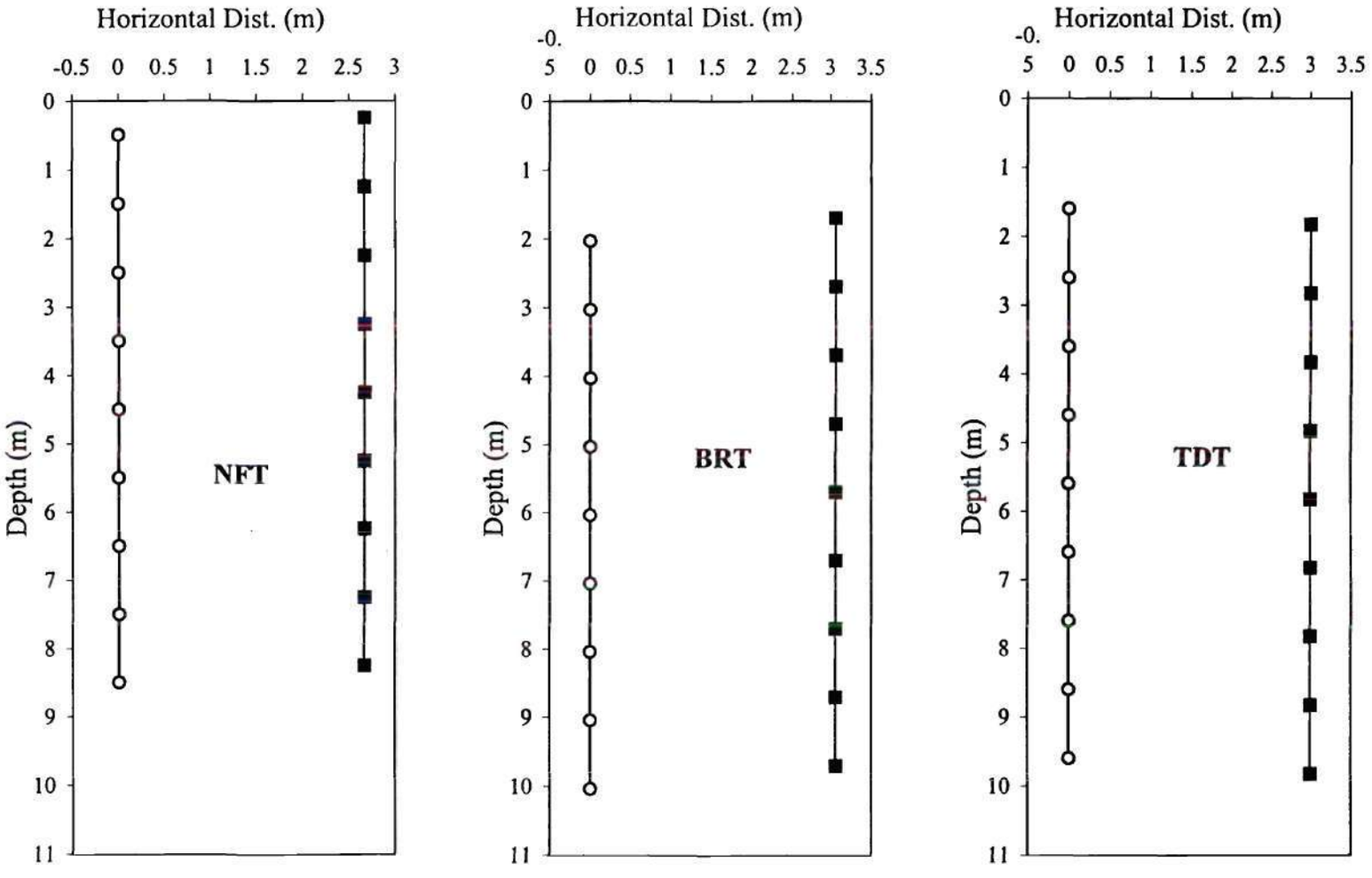

Fig. 4 Geometry of the 3 experimental setups

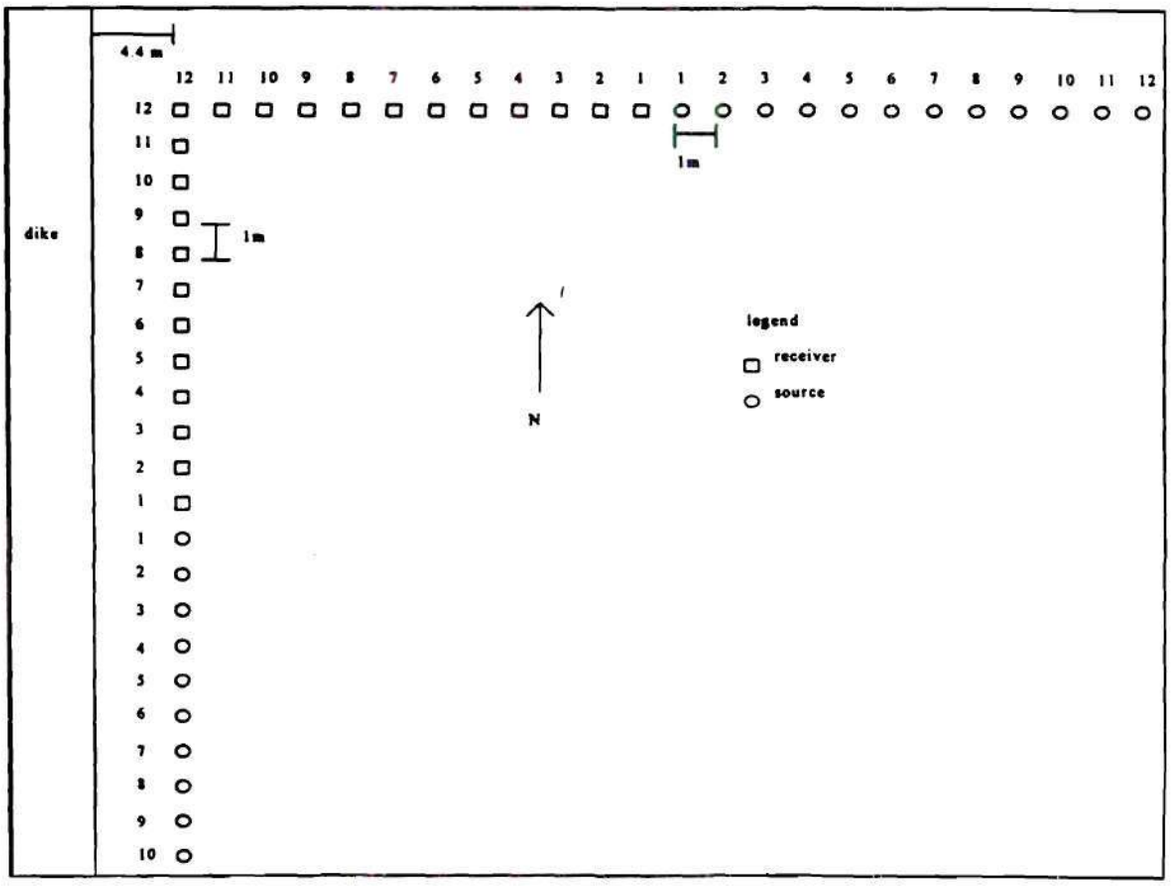

Fig. 5 Seismic reflection / refraction survey on the berm

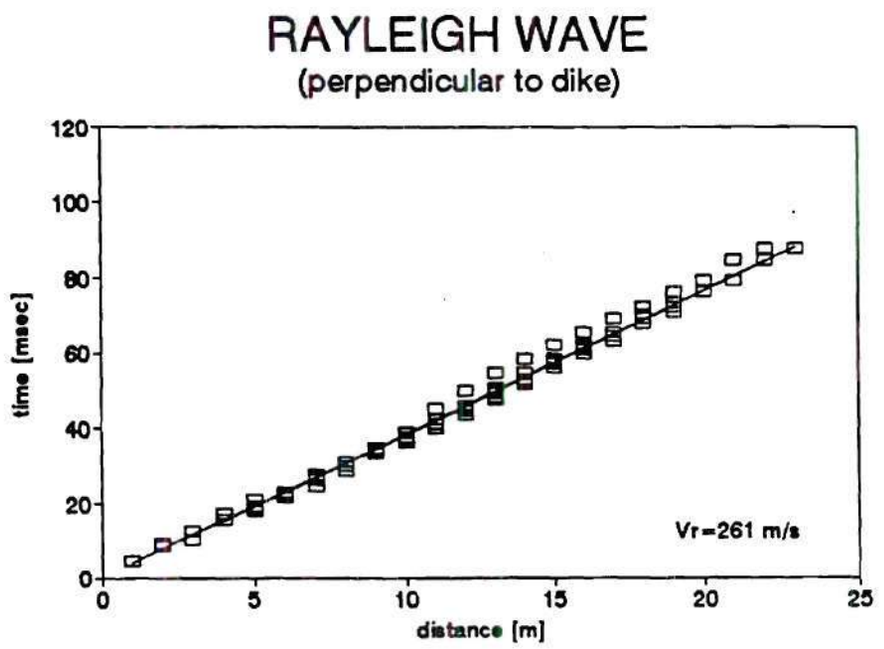

Fig. 6 Seismic reflection / refraction survey on the berm: perpendicular to dam (a) First arrival P-wave; (b) Raleigh wave arrival

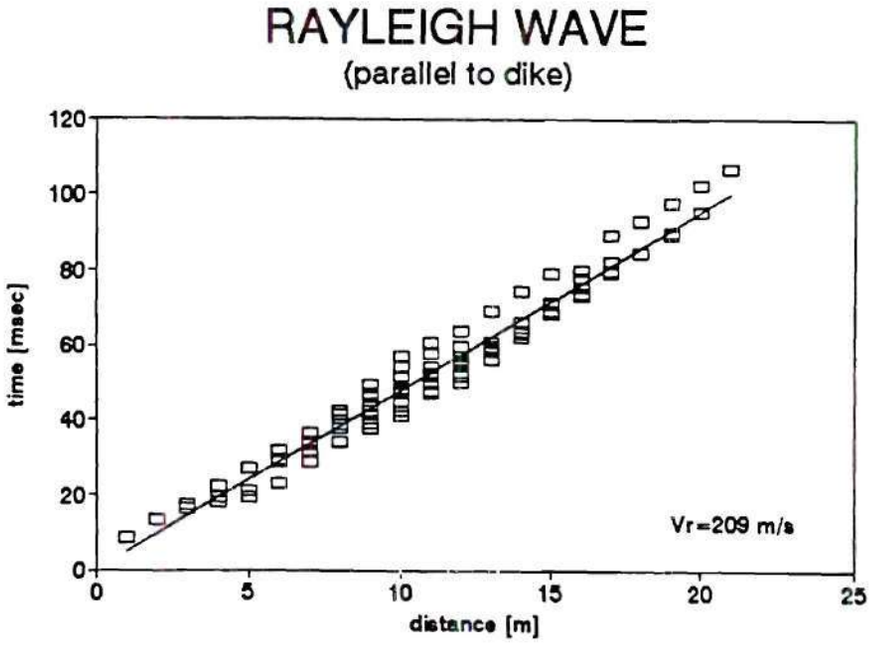

Fig. 7 Seismic reflection / refraction survey on the berm: parallel to dam (a) First arrival P-wave; (b) Raleigh wave arrival

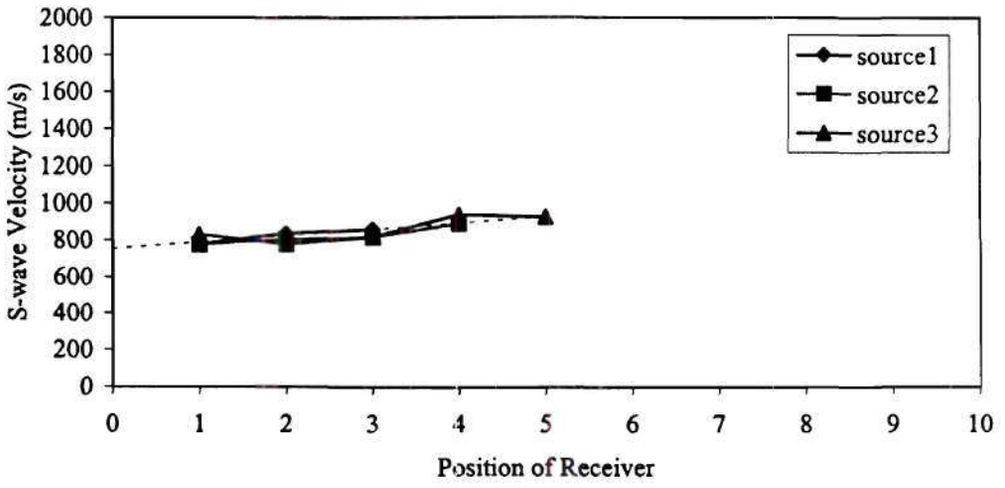

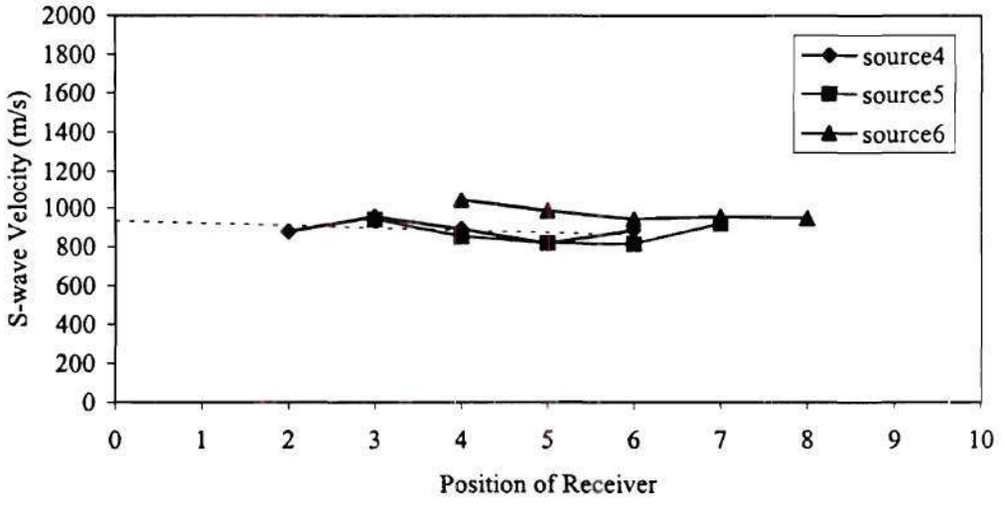

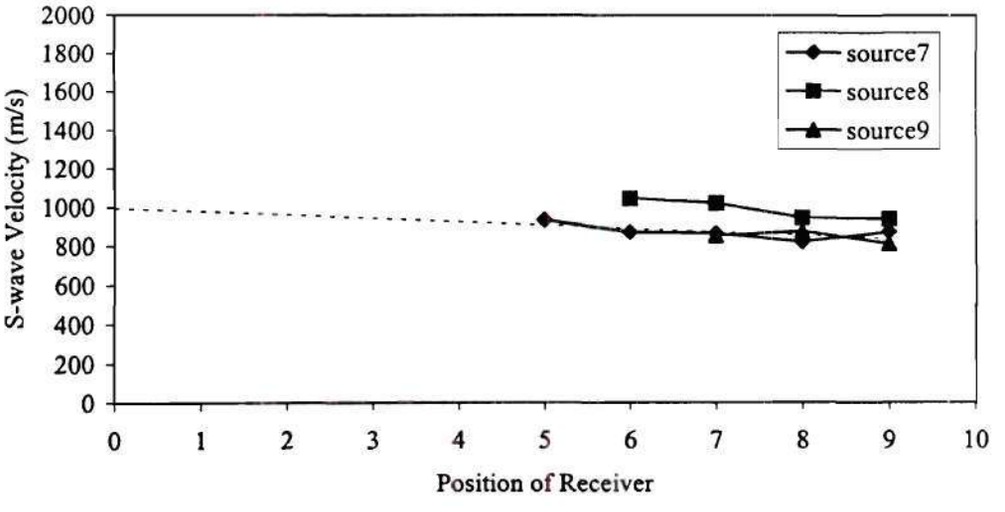

Fig. 8.a P-wave velocity shadows BRT test

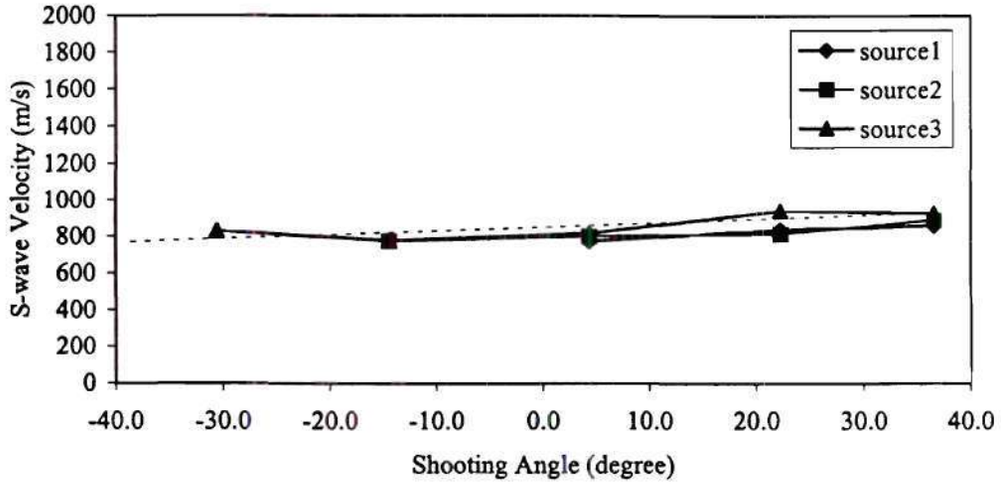

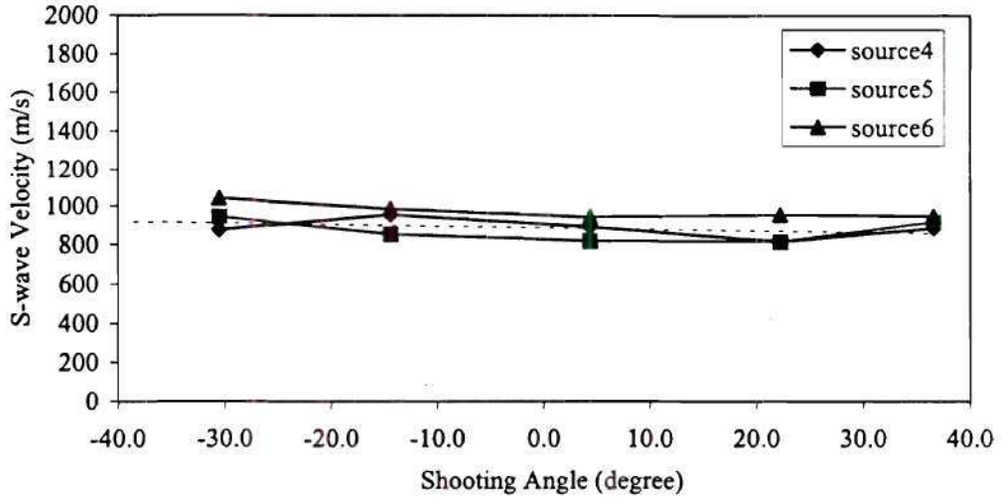

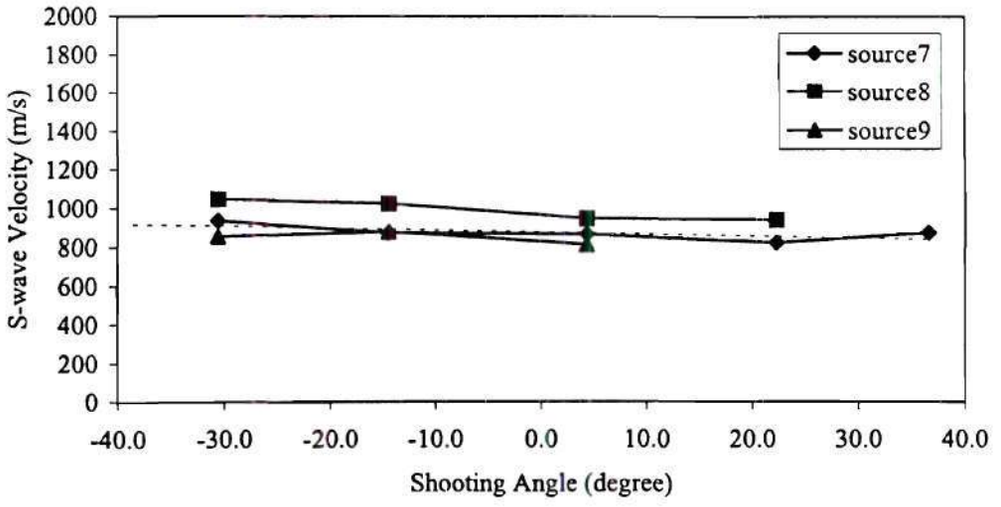

Fig. 8.b P-wave velocity vs. shooting angle. BRT test

(Ishihara, 1998)

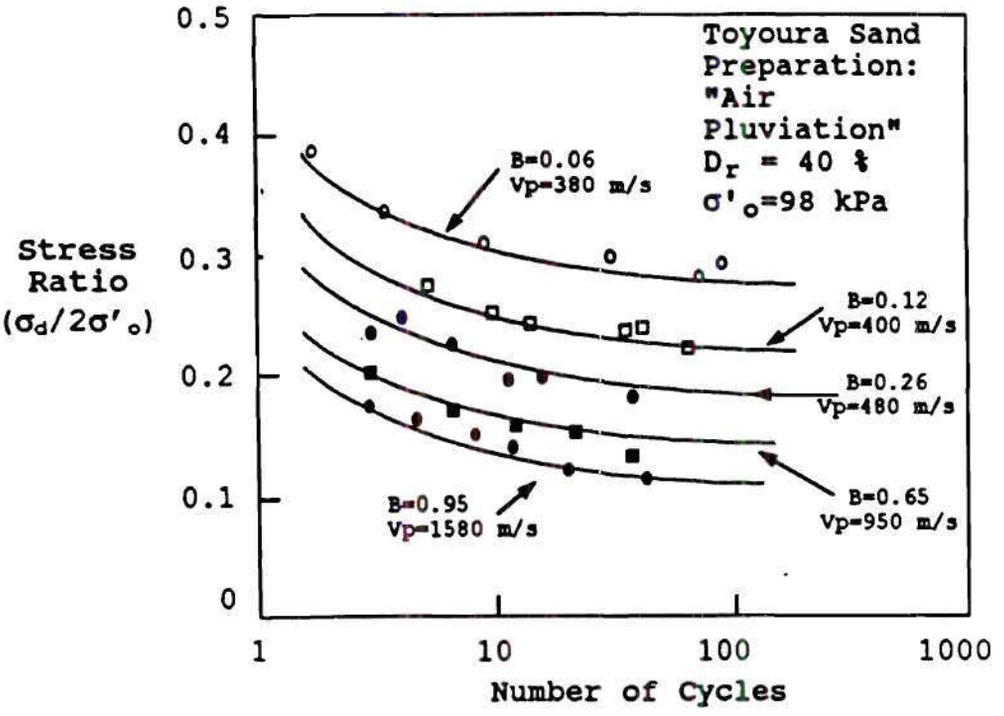

(Head, 1986)

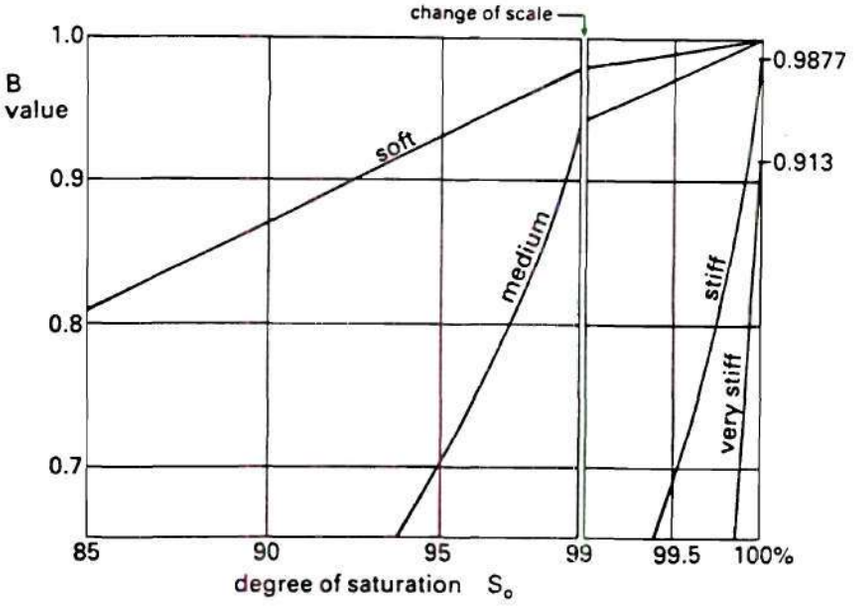

Fig. 9 Relationships between S-wave velocity and Skempton's B parameter (Ishihara, 1998 and Head, 1986)

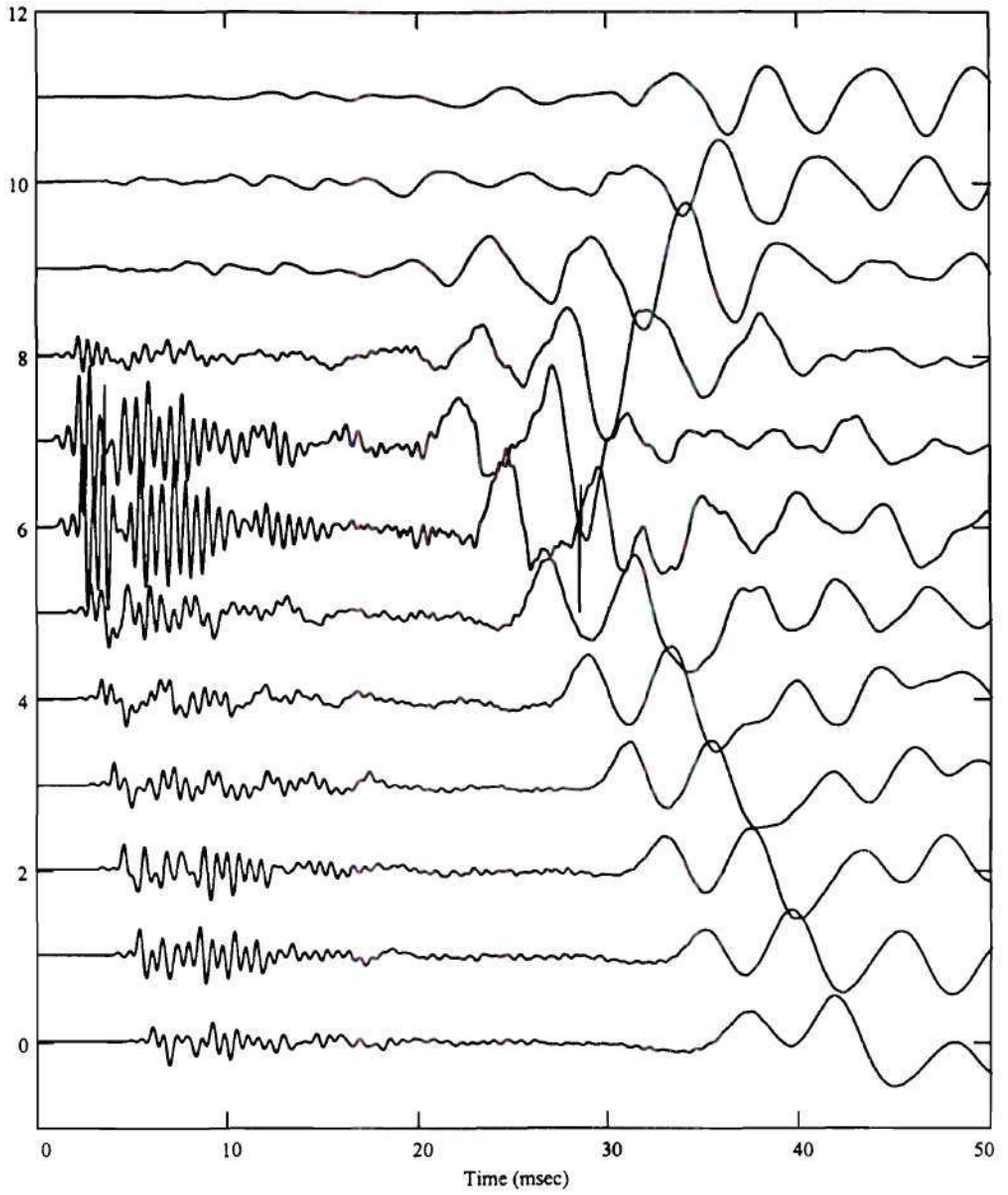

Fig. 10 Typical record registered during the test

NFT		BRT		TDT	
Depth (m	Vs(m/s)	Depth (m	Vs(m/s)	Depth (m	Vs(m/s)
0.375	102.75	2.2	141.23	1.715	156.71
1.375	121.89	3.2	148.02	2.715	184.59
2.375	120.25	4.2	159.52	3.715	192.87
3.375	126.79	5.2	86.00	4.715	104.11
4.375	97.87	6.2	82.76	5.715	167.16
5.375	106.42	7.2	80.81	6.715	116.17
6.375	98.59	8.2	85.05	7.715	97.06
7.375	112.20	9.2	79.56	8.715	114.40
8.375	119.72	10.2	81.02	9.715	139.94

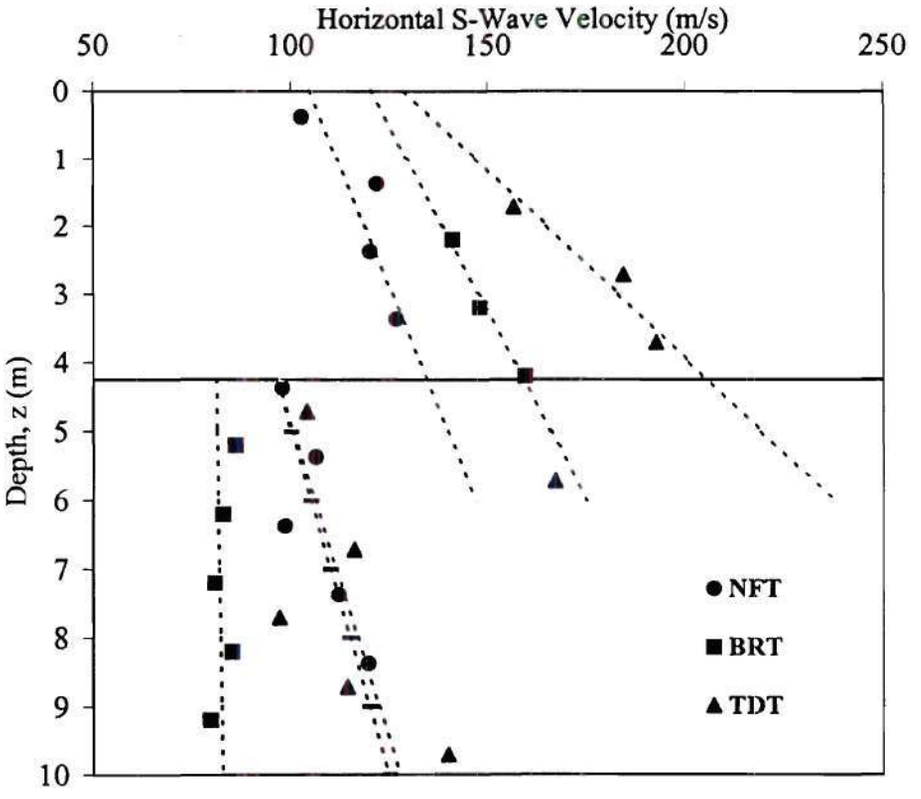

Fig. 11 S-wave velocity (horizontal rays) vs. depth for all tests

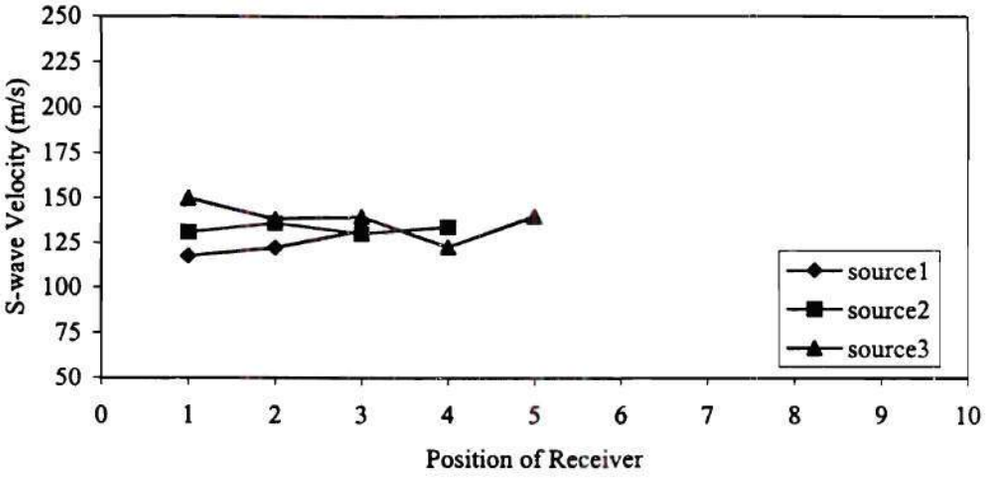

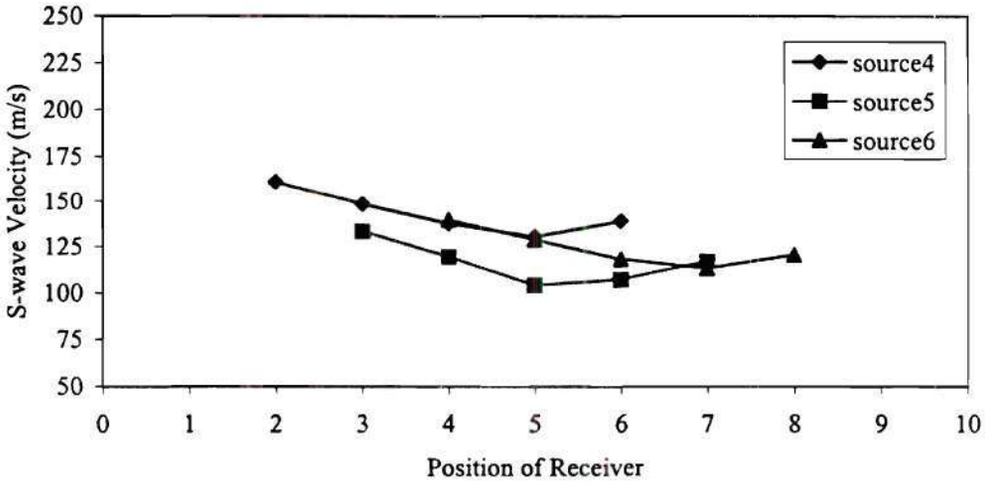

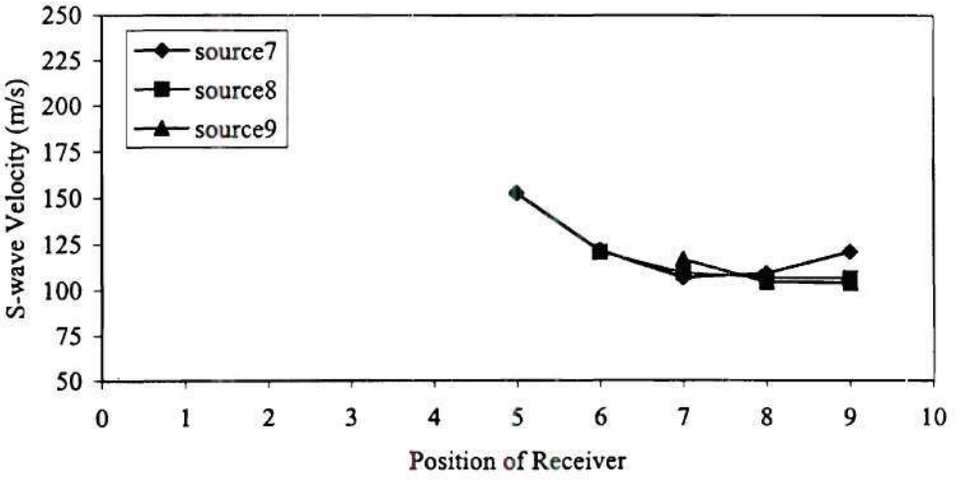

Fig. 12.a S-wave velocity shadows for the Natural Field

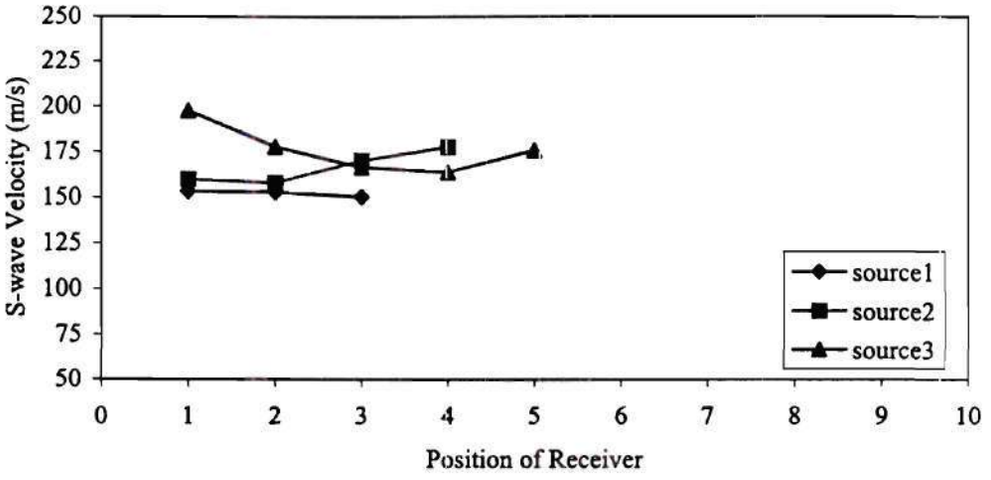

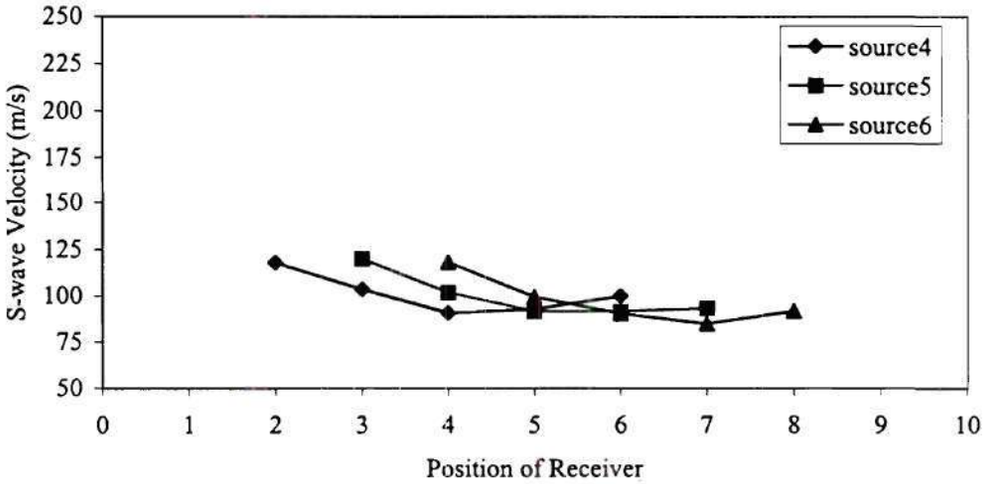

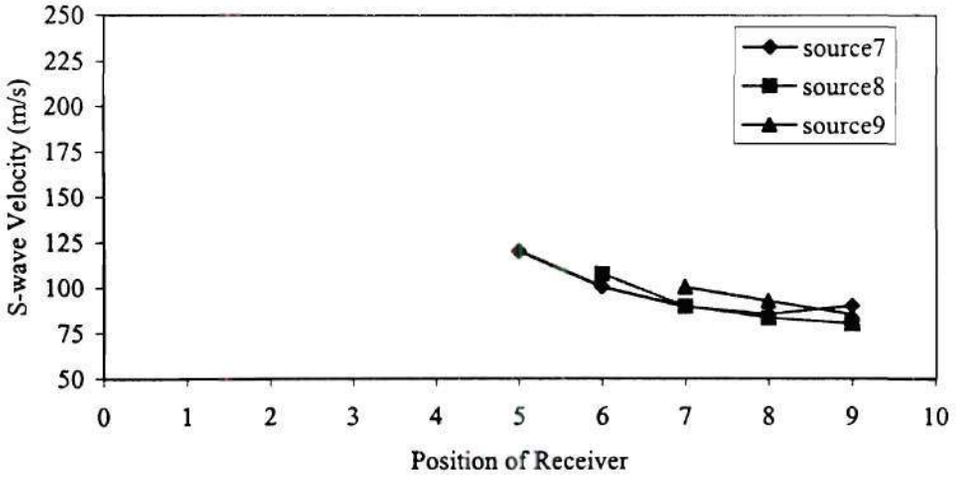

Fig. 12.b S-wave velocity shadows for the Berm

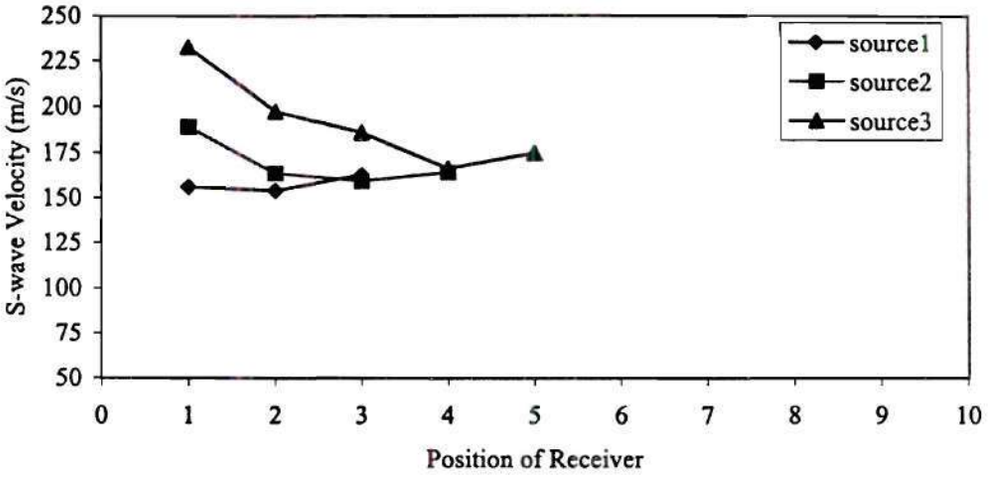

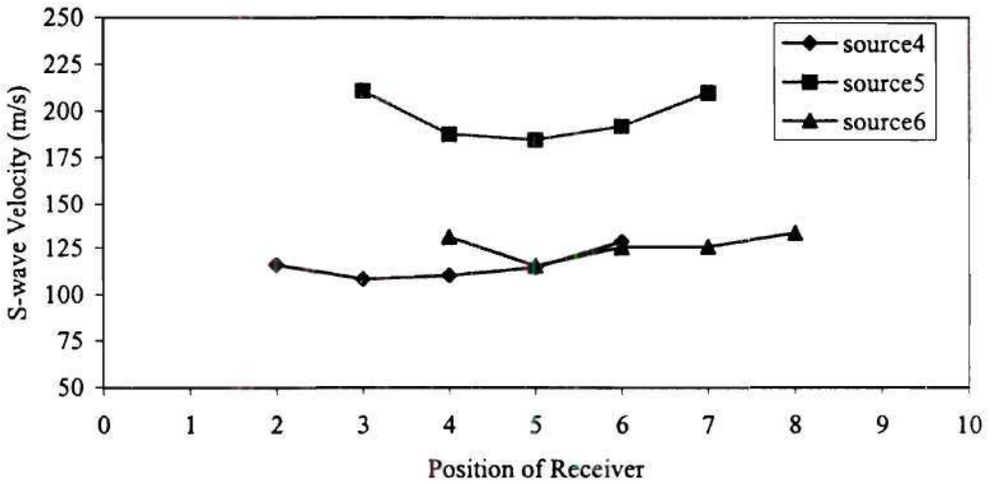

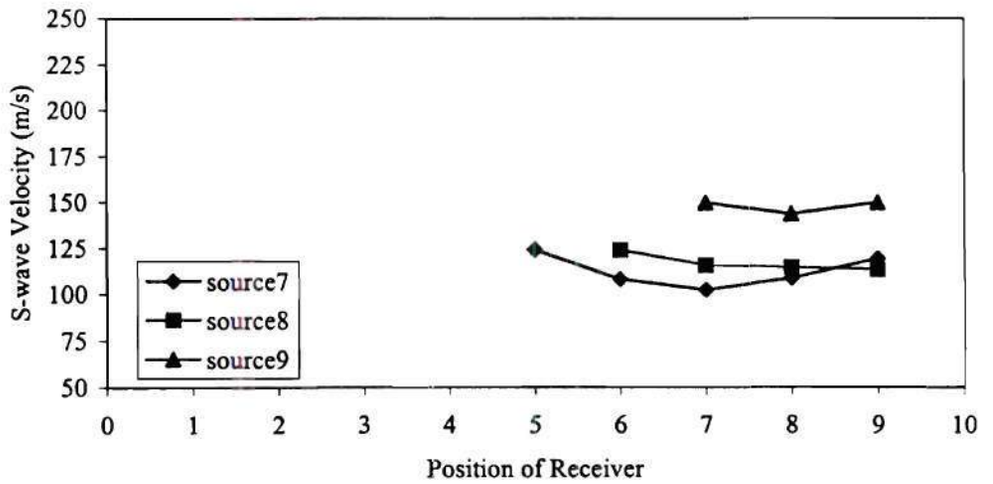

Fig.12.c S-wave velocity shadows for the Top of Dam

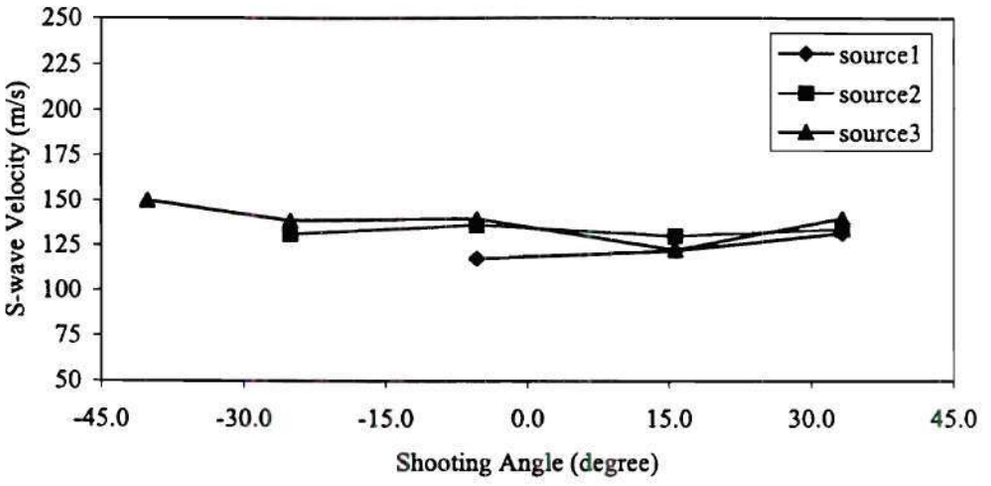

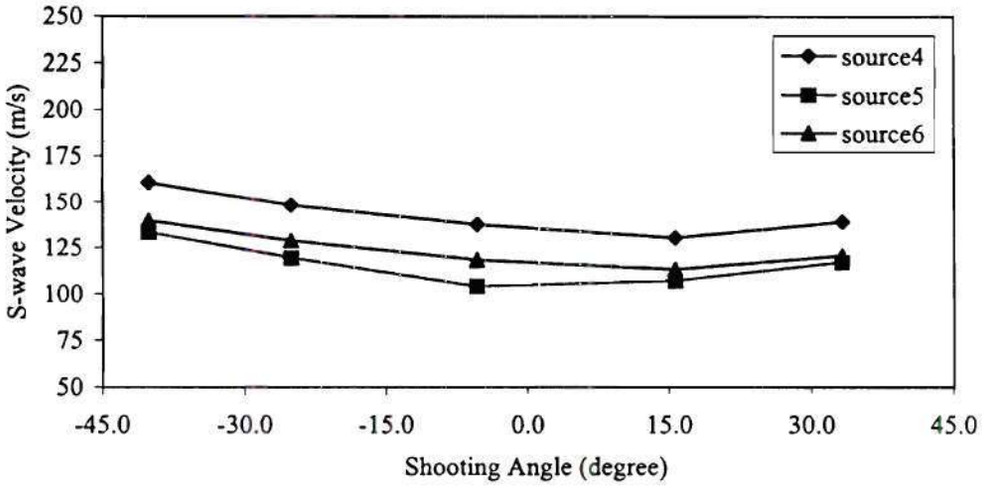

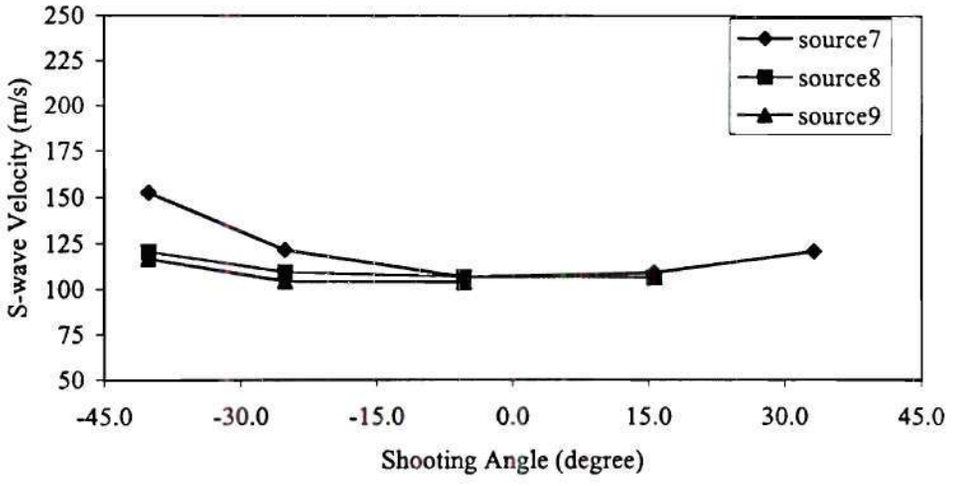

Fig. 13.a S-wave velocity vs. shooting angle for the Natural Field

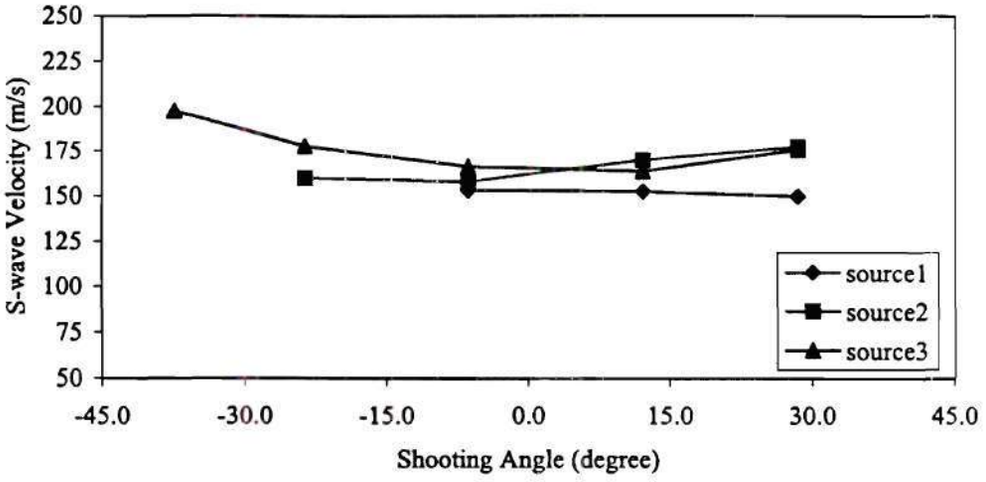

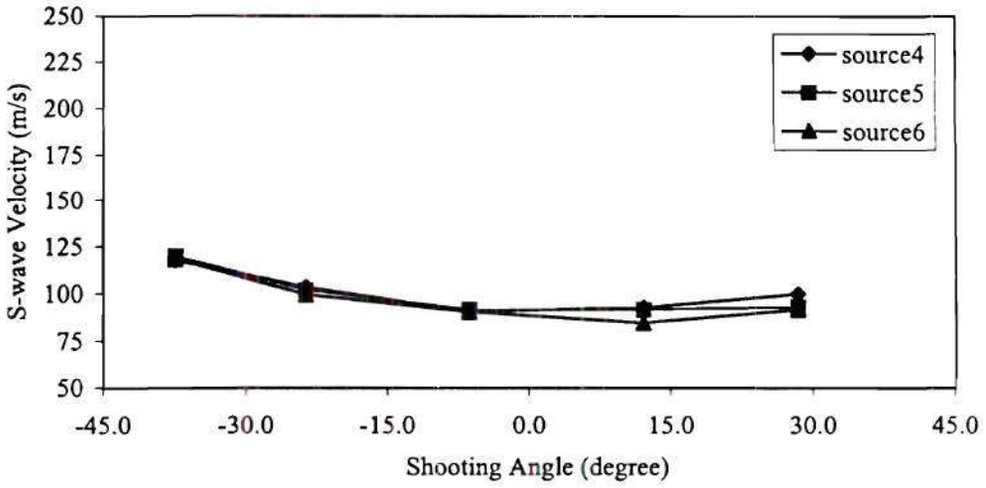

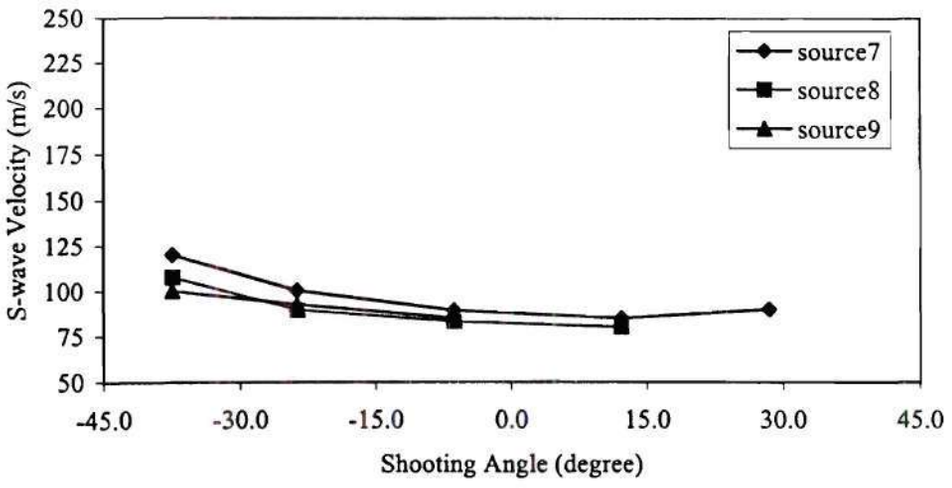

Fig. 13.b S-wave velocity vs. shooting angle for the Berm

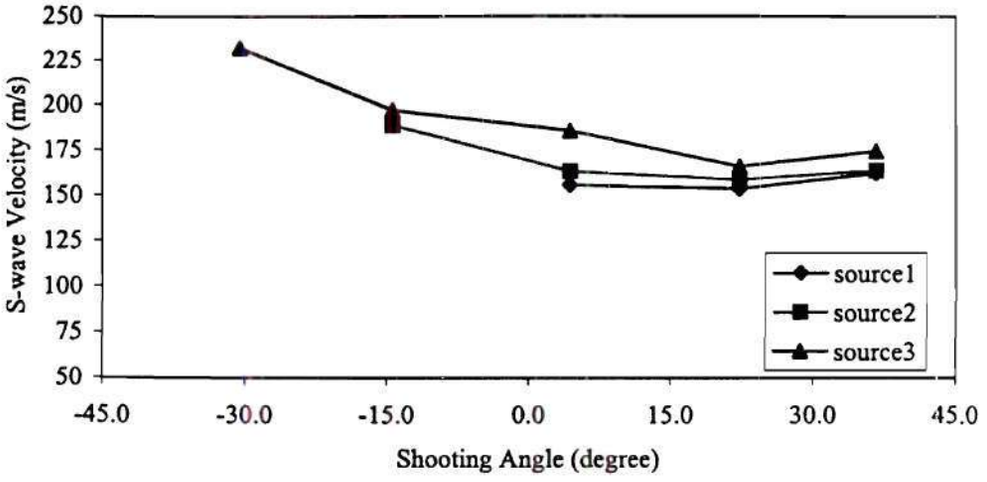

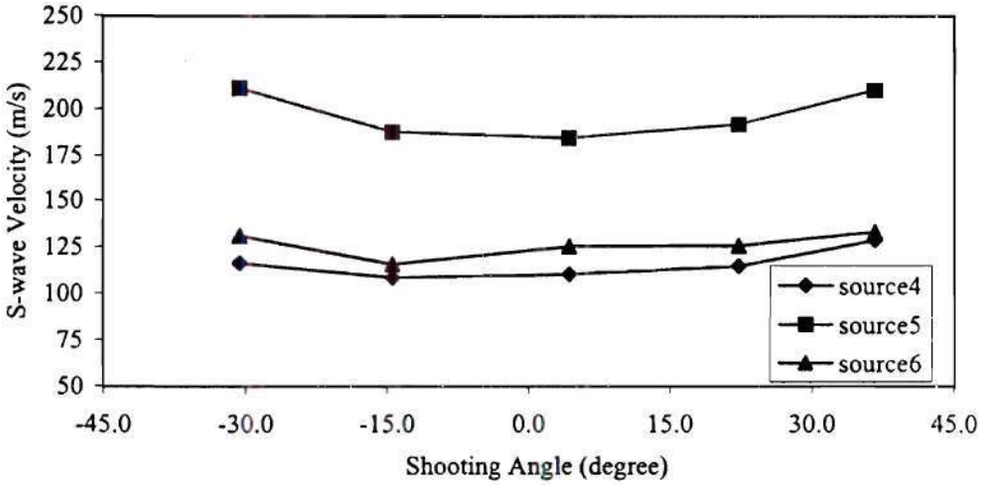

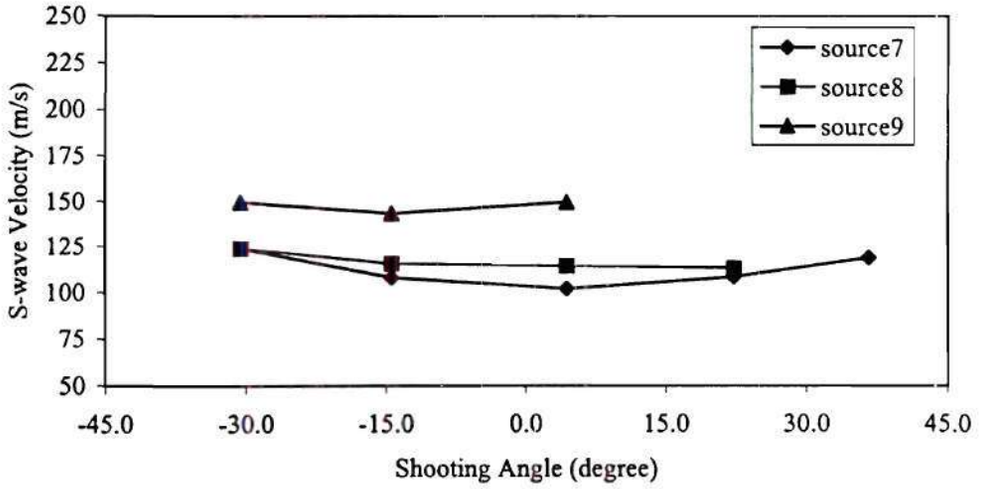

Fig.13.c S-wave velocity vs. shooting angle for the Top of Dam

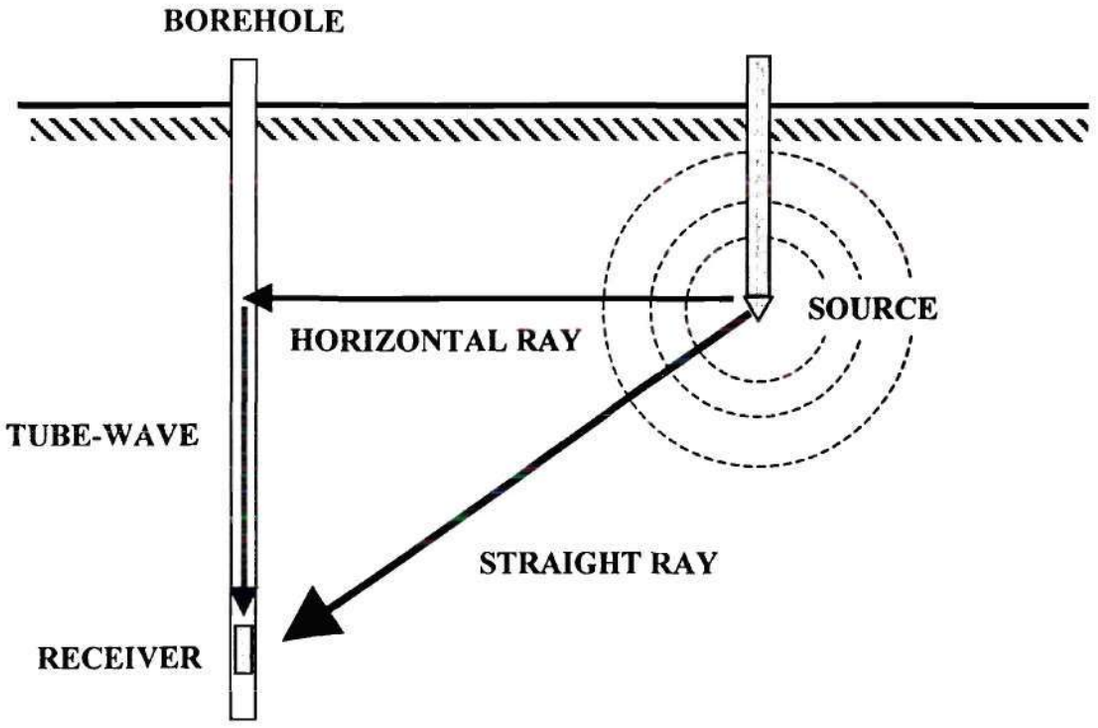

Fig. 14 Model for the error in travel times

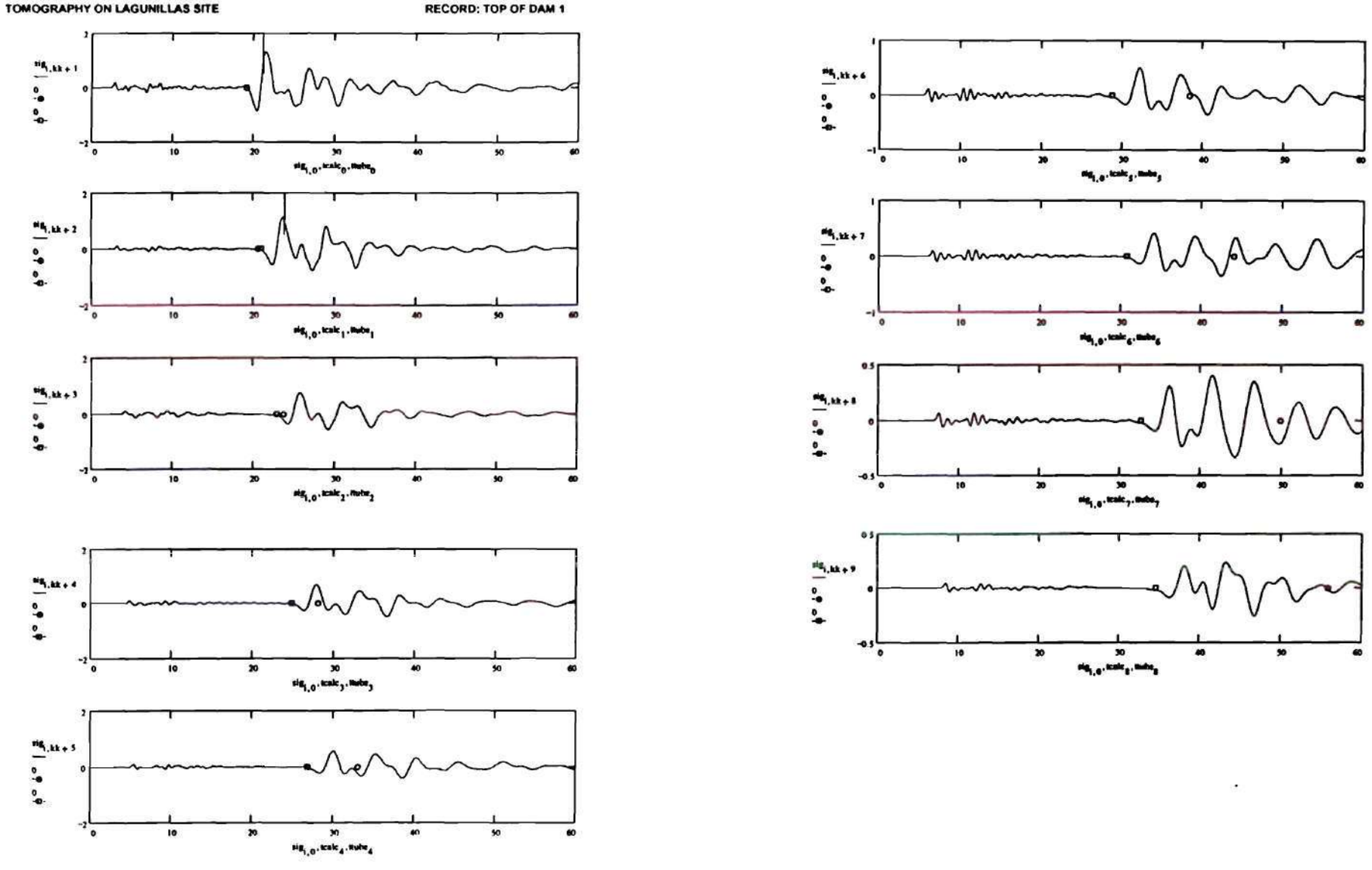

Fig. 15 Definition of the tube-wave arrival (The square represents the prediction for the arrival of the tube-wave, the circle is the estimation of the S-wave arrival based on average horizontal velocities)

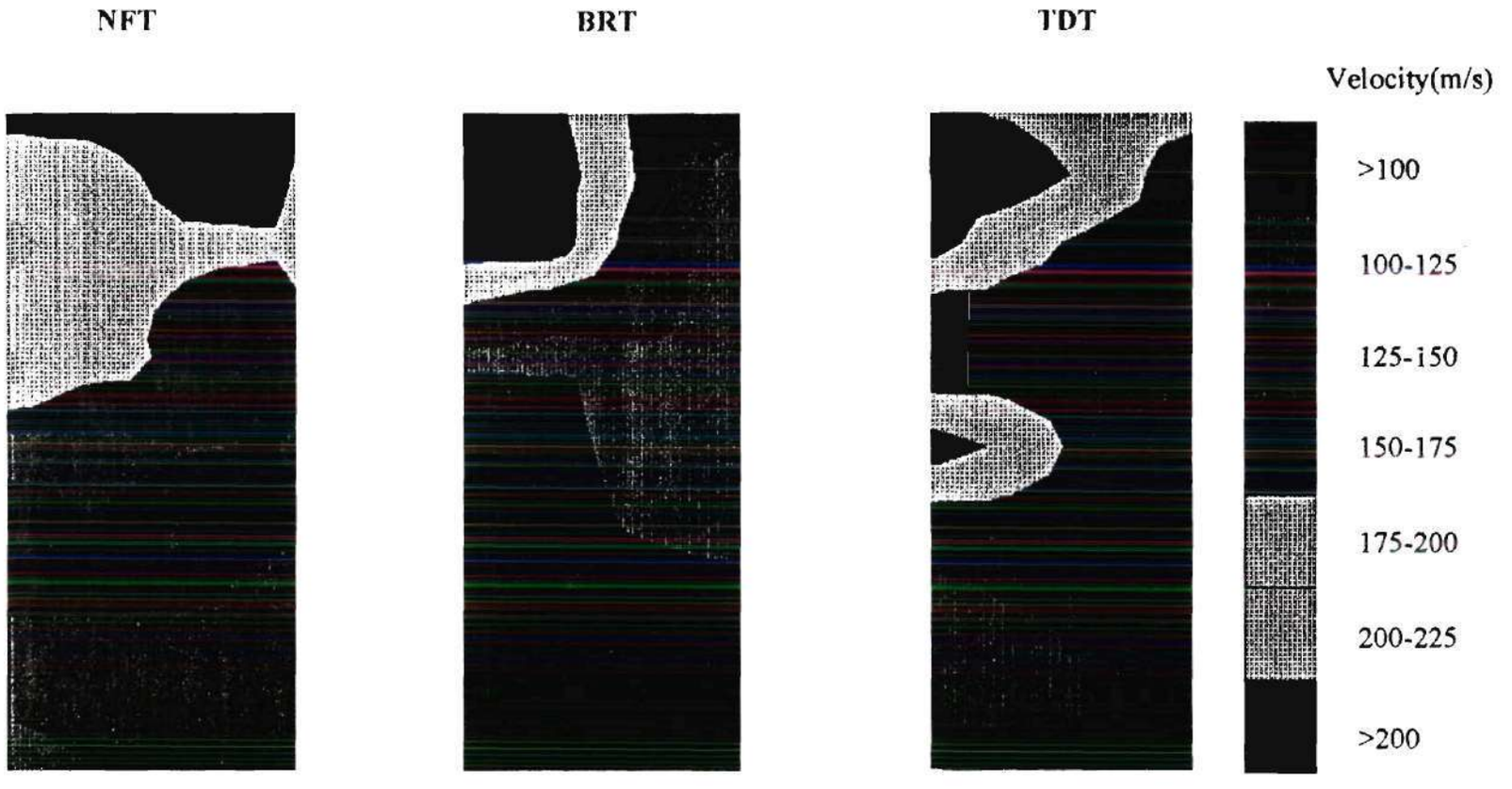

Fig. 16 Tomographic images of the S-wave velocity with global smoothing

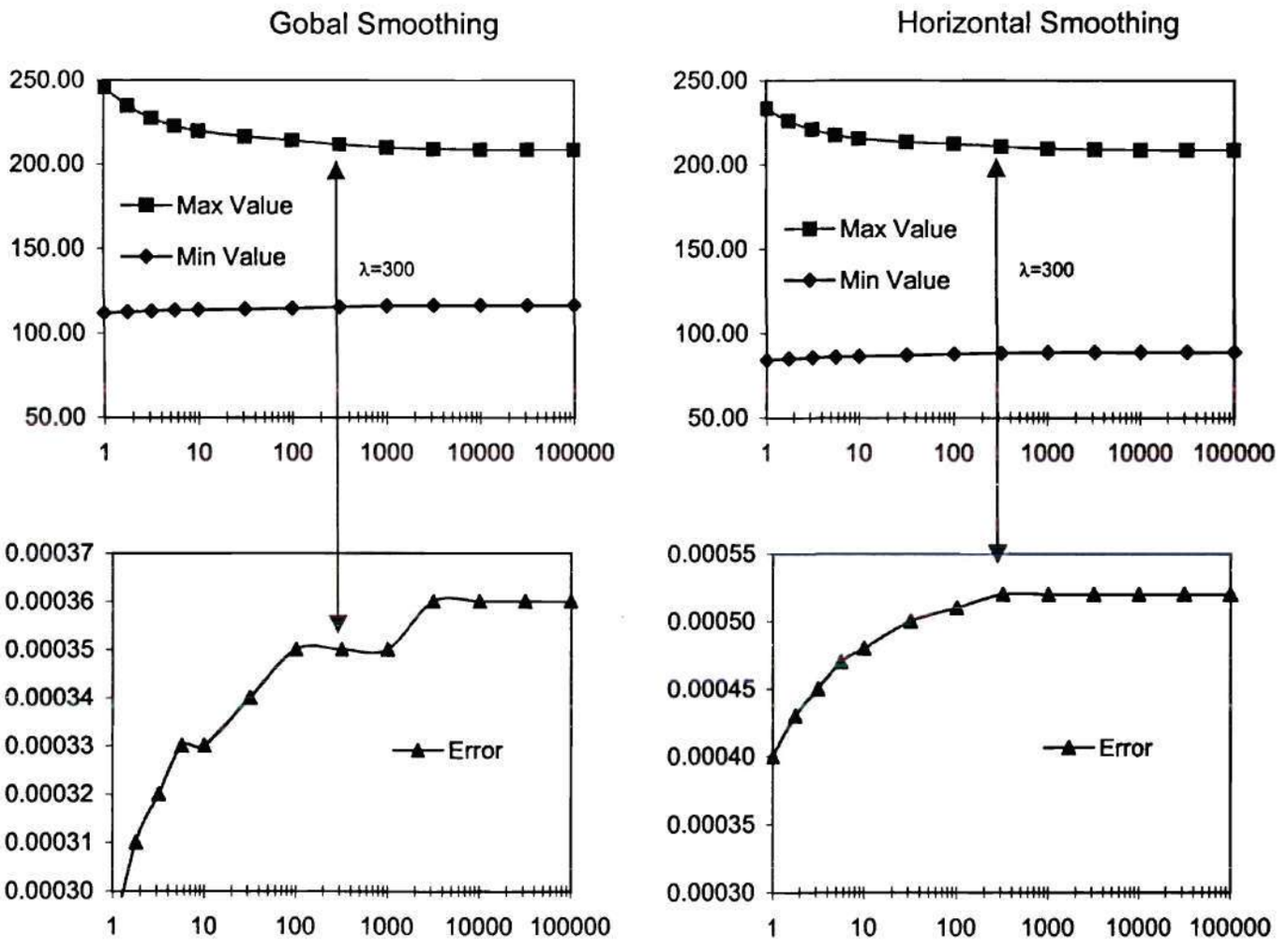

Fig. 17 Definition of the regularization parameter λ

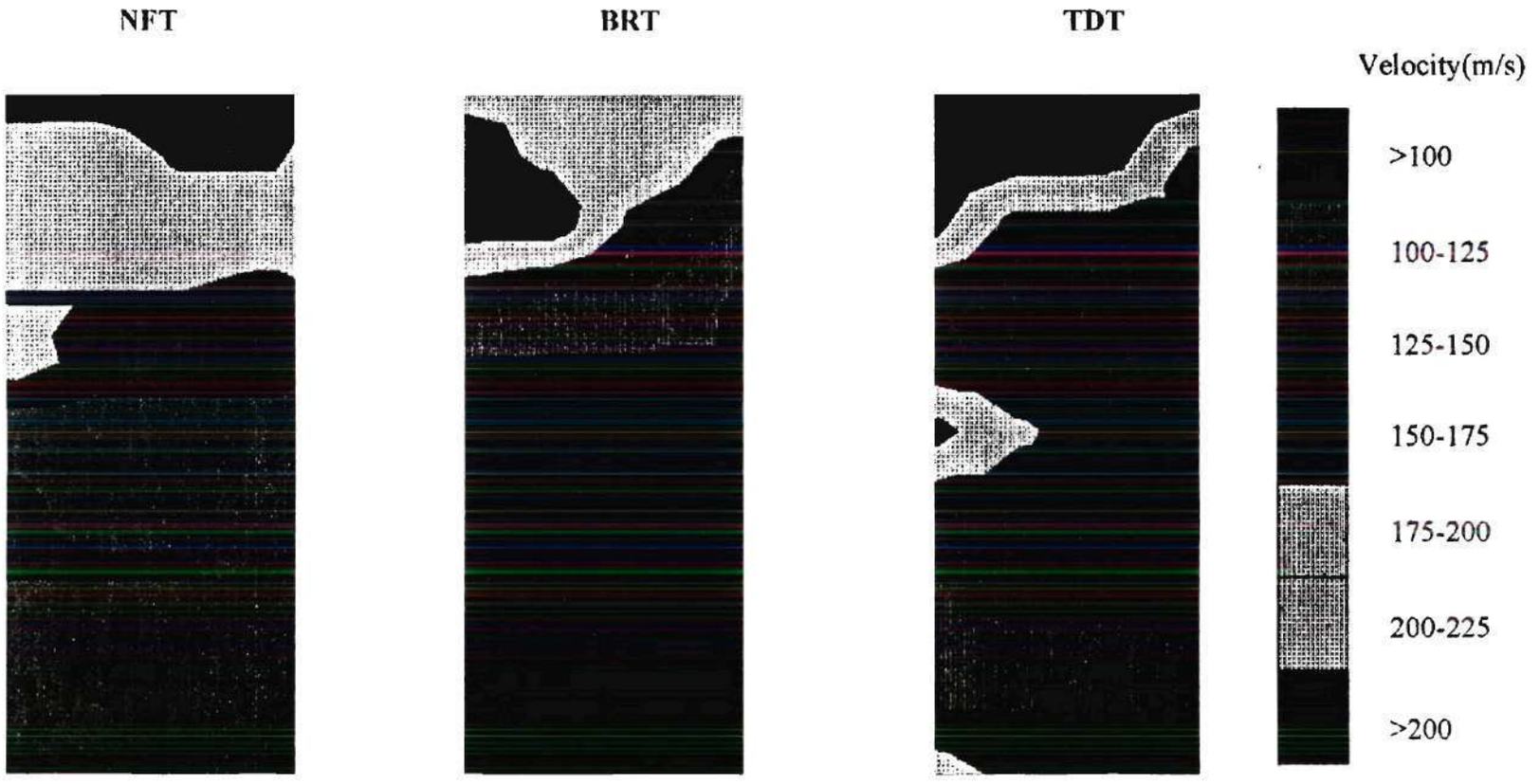

Fig. 18 Tomographic images of the S-wave velocity with horizontal smoothing

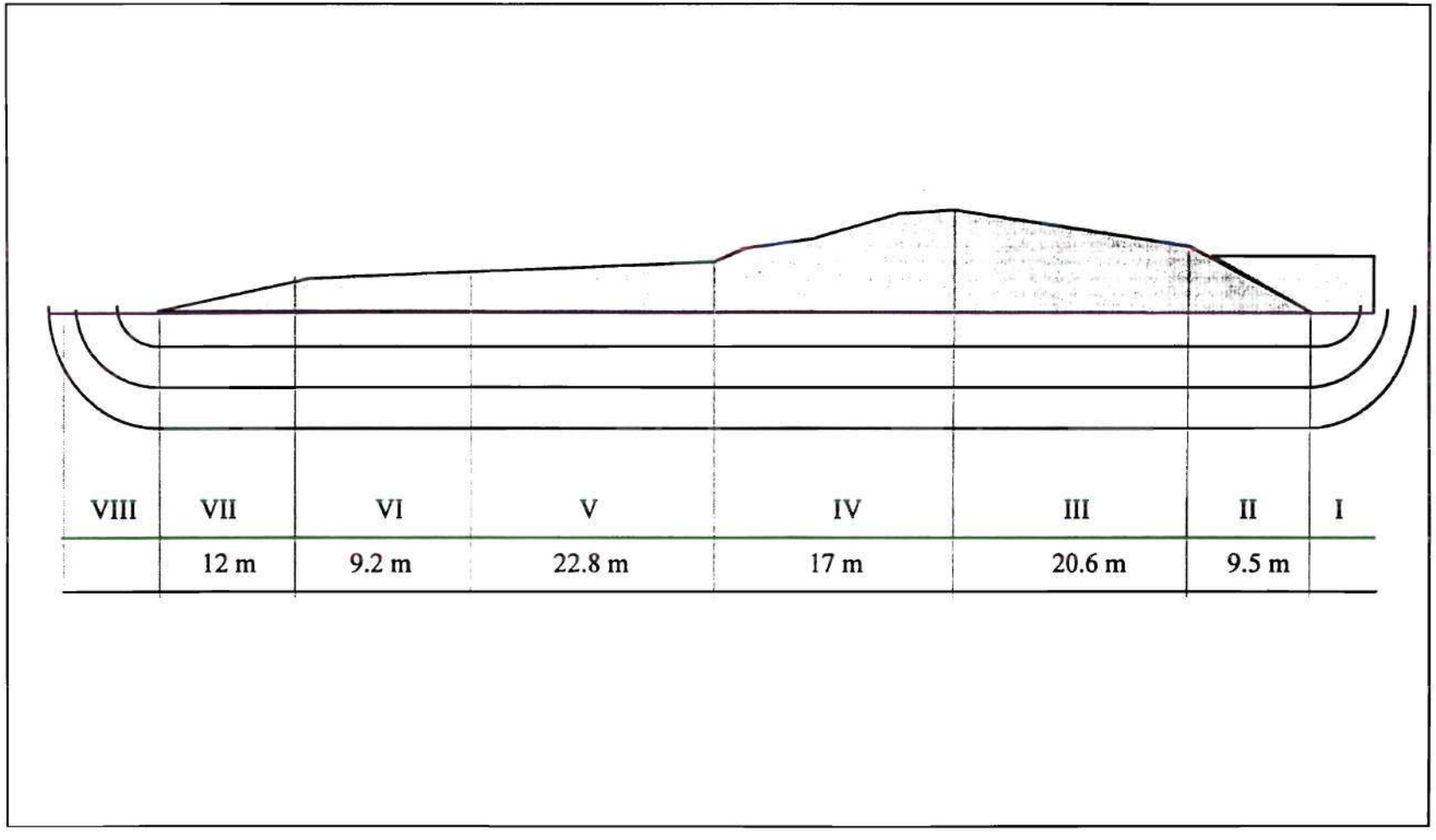

Fig. 19 Flownet - Method of fragments

FLOWNET COMPUTATIONS
METHOD OF FRAGMENTS

Fragment	I	II	III	IV	V	VI	VII	VIII
L (m)		9.5	20.6	17	22.8	9.2	12	
Δh (m)	0	0.448	0.972	0.803	1.076	0.435	0.566	0
hT (m)	14.3	13.852	12.88	12.077	11.001	10.566	10	10

Depth (m)	Piezometric Pressure							
1	53	48.52	38.8	30.77	20.01	15.66	10	10
2	63	58.52	48.8	40.77	30.01	25.66	20	20
3	73	68.52	58.8	50.77	40.01	35.66	30	30
4	83	78.52	68.8	60.77	50.01	45.66	40	40
5	93	88.52	78.8	70.77	60.01	55.66	50	50
6	103	98.52	88.8	80.77	70.01	65.66	60	60
7	113	108.52	98.8	90.77	80.01	75.66	70	70
8	123	118.52	108.8	100.77	90.01	85.66	80	80
9	133	128.52	118.8	110.77	100.01	95.66	90	90
10	143	138.52	128.8	120.77	110.01	105.66	100	100

Depth (m)	Total Stress							
1	58	71.32	149.86	136.55	88.7	76.16	51.08	15
2	73	86.32	164.86	151.55	103.7	91.16	66.08	30
3	88	101.32	179.86	166.55	118.7	106.16	81.08	45
4	103	116.32	194.86	181.55	133.7	121.16	96.08	60
5	118	131.32	209.86	196.55	148.7	136.16	111.08	75
6	133	146.32	224.86	211.55	163.7	151.16	126.08	90
7	148	161.32	239.86	226.55	178.7	166.16	141.08	105
8	163	176.32	254.86	241.55	193.7	181.16	156.08	120
9	178	191.32	269.86	256.55	208.7	196.16	171.08	135
10	193	206.32	284.86	271.55	223.7	211.16	186.08	150

Depth (m)	Effective Stress							
1	5	22.8	111.06	105.78	68.69	60.5	41.08	5
2	10	27.8	116.06	110.78	73.69	65.5	46.08	10
3	15	32.8	121.06	115.78	78.69	70.5	51.08	15
4	20	37.8	126.06	120.78	83.69	75.5	56.08	20
5	25	42.8	131.06	125.78	88.69	80.5	61.08	25
6	30	47.8	136.06	130.78	93.69	85.5	66.08	30
7	35	52.8	141.06	135.78	98.69	90.5	71.08	35
8	40	57.8	146.06	140.78	103.69	95.5	76.08	40
9	45	62.8	151.06	145.78	108.69	100.5	81.08	45
10	50	67.8	156.06	150.78	113.69	105.5	86.08	50

Top	Depth (m)	Berm	Depth (m)	Natural	Depth (m)
111.06	1	68.69	1	5	1
116.06	2	73.69	2	10	2
121.06	3	78.69	3	15	3
126.06	4	83.69	4	20	4
131.06	5	88.69	5	25	5
136.06	6	93.69	6	30	6
141.06	7	98.69	7	35	7
146.06	8	103.69	8	40	8
151.06	9	108.69	9	45	9
156.06	10	113.69	10	50	10

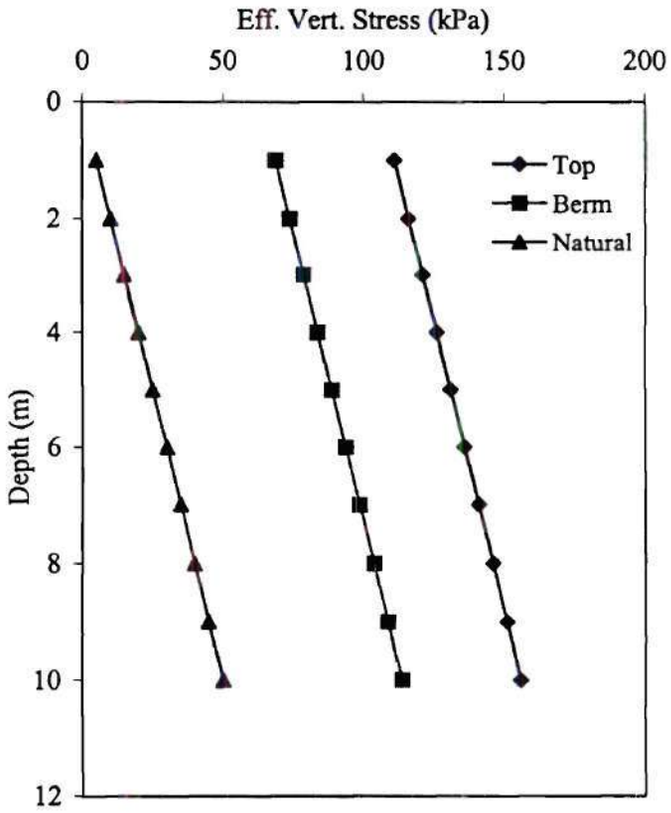

Table 2. Typical values for α and β

Type of Material	α (kPa)	β
Tia Juana Soil	36.46	0.347
Barco Sand	91.34	0.250
Silica Sand	112.56	0.176
Silica/Kaolin Pellets	56.08	0.250
Silica/Kaolin Pellets	79.06	0.330
Lagunillas Silt	54.93	0.258
Silica Fluor	30.00	0.309
Kaolinite	41.00	0.301
Steel Spheres	170.74	0.140
Lead Shots	56.95	0.250

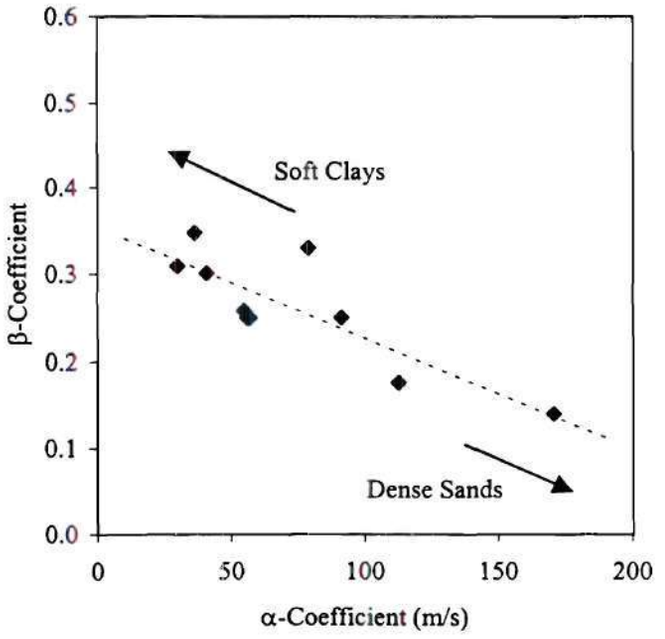

$$\beta = 0.35 - \alpha / 800$$

α is in [m/s] for a mean stress of 1 kPa

Fig.20 Typical values for α and β coefficients

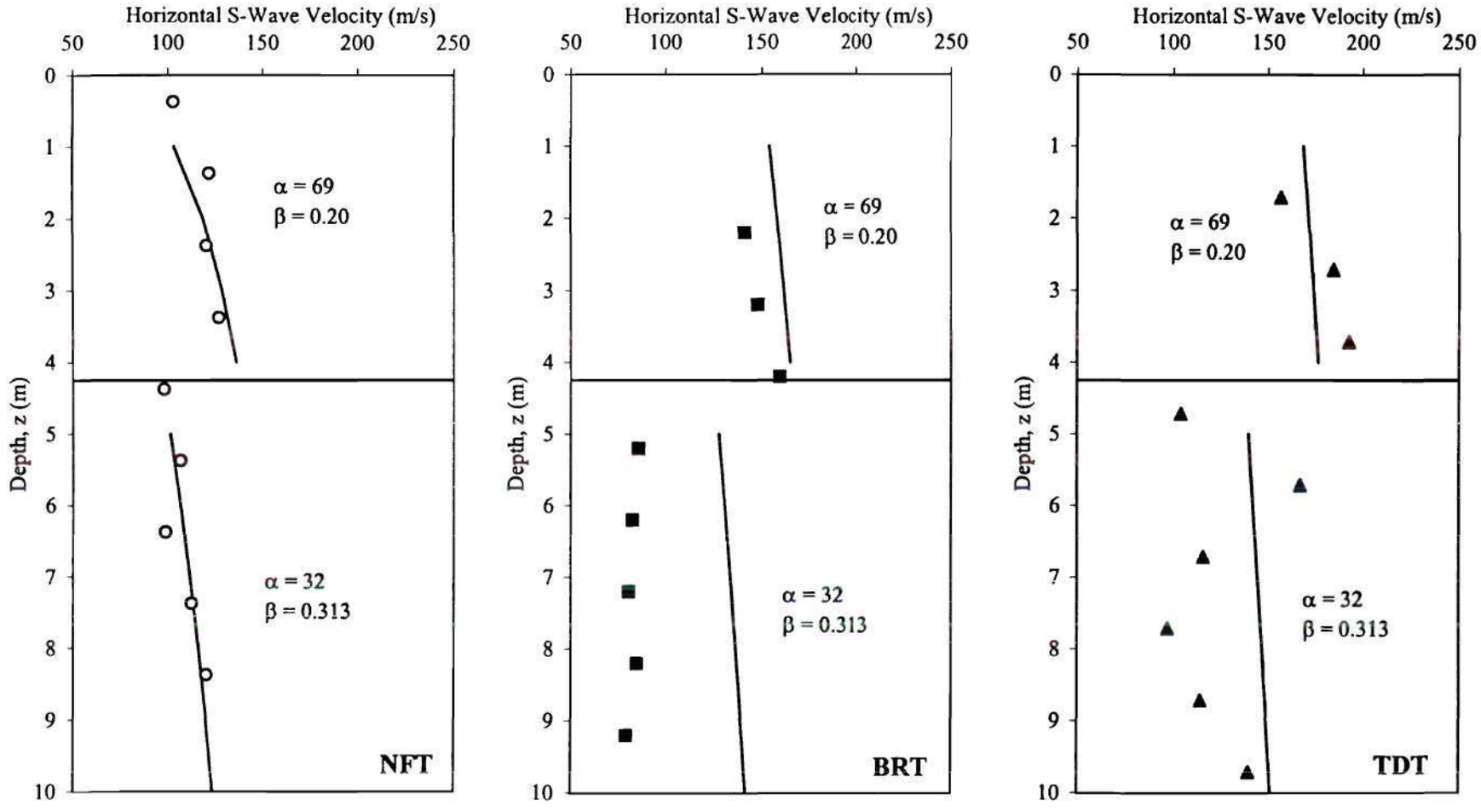

Fig. 21 Shear-wave velocity distribution (from horizontal rays) for the 3 tests. Solid lines represent the model fit with the α and β corresponding to the NFT

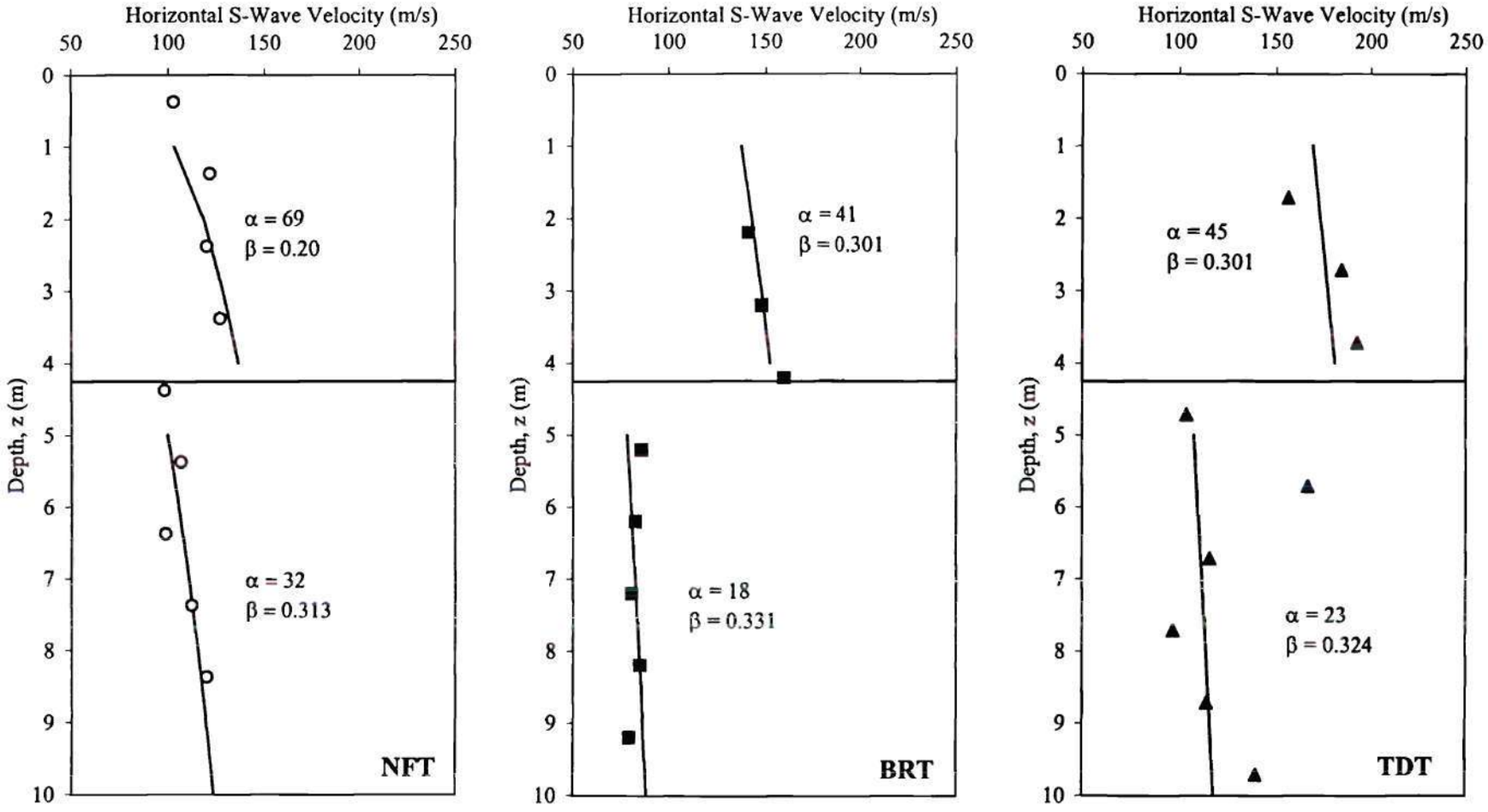

Fig. 22 Shear-wave velocity distribution (from horizontal rays) for the 3 tests. Solid lines represent the model fit with the α and β corresponding to each test

E-20-F09

Georgia Institute of Technology
School of Civil and Environmental Engineering
Geosystems Department
August 1999

DESIGN OF A FIELD SOURCE OF MECHANICAL WAVES

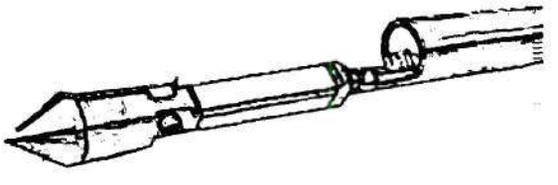

SUMMARY

Crosshole tomography is highly sensitive to the noise level of the recorded signals. Although, signal process can be used to reduce noise, it also adds information to the system. Therefore, the quality of the data is affected by the signal processing. In this case, it is strongly suggested to spend more time in the design of the test, and when it is possible, to improve the quality of the hardware. Standard geophones are sensitive enough for the purpose of crosshole testing; for that reason, an additional effort was done to produce a new kind of source to improve the emission of mechanical waves. According to the design parameters, the source should be capable of: (1) produce shear-waves; (2) eliminate the need for a cased borehole; (3) work below the water table; and (4) low maintenance

Two different prototypes of field sources have been designed in order to improve the quality of the data. The first one is a pneumatic source, and the second one is a battery-operated electrical source. Both prototypes are designed to be driven into the ground with standard CPT equipment.

1. SOURCE I - PNEUMATIC SOURCE

1.1 Description

The first prototype consists on a pneumatic vibrator assembled inside a cone-type probe (see Appendix A). The vibrator is springless with a double-impact match-plate. These patented features provide trouble-free operation, which reduces maintenance and inconveniences from vibrator spring breakage. The vibrator produces a continuous sinusoidal wave that is transmitted to the tip of the cone.

Characteristics of the vibrator:

- Air Consumption @ 4.1 bar (60 psig) = 3.8 liters per min.
- Frequency @ 4.1 bar (60 psig) 14,100 blows/min
- 3/8" (1.0 cm) hose fitting.

1.2 Advantages / Disadvantages

The advantages of using this type of source are:

- Robust and low maintenance design
- Relative easy to operate (only requires compressed air)
- Propitiates the use of cross correlation to determine delay between signals

On the other hand, the disadvantages of this type are:

- The triggering mechanism is more complex
- Is difficult to control the air pressure during the test

1.3 Usage / Maintenance

The source should be connected to a source of compressed air (tank or compressor) using a 1/4" Teflon/Nylon hose with a 3/8" pressure connection. The minimum operating pressure of the vibrator should be 40 psi (280 kPa). Before using the source, the internal part of the vibrator should be lubricated using the proper lubricant oil. After use, the vibrator should be checked to assure that the air vents are free from clogs.

Field Experience

The Source I has already been tested in the field. The tests consisted in driving the source up to 2.00 m beneath the ground surface, and measuring the shear wave with buried and on surface geophones. The maximum horizontal separation from the source measured in this test was 6.6m (20 ft). The overall performance of the source was very good. In the case of the geophones placed on surface, the recorded signals were very sinusoidal, and for the buried geophones, the received signal was very "harmonic" (See Fig.1).

In conclusion, cross-correlation procedures can be easily applied to determine the delay time between geophones.

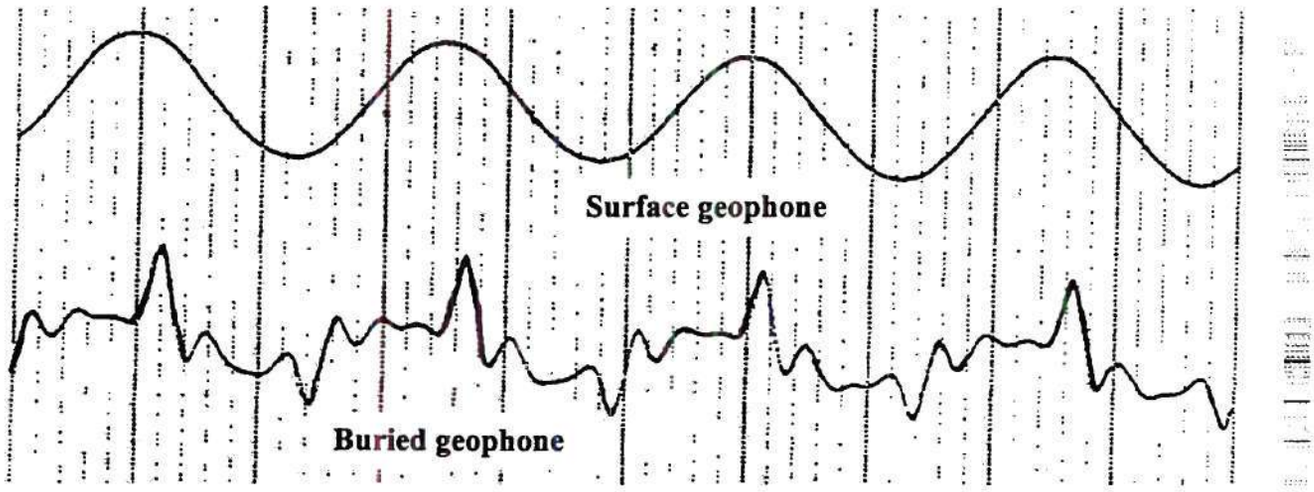

Fig.1 Signals recorded in the field test for the source I

2. SOURCE II - ELECTRIC SOURCE

2.1 Description

Even though the exterior design of this source is similar to the Source I, there are some fundamental differences: (1) this source uses an electric solenoid that delivers the energy to the cone-tip; (2) the stroke in this source is not continuous; (3) the overall length of this probe is smaller than the pneumatic one, which reduces the friction component during extraction and (4) space distribution inside the probe gives more freedom to employ different types of trigger. So far, the probe has been tested with an inertial type of trigger.

Characteristics of the solenoid:

- Coil Voltage: 12 volt (DC) - Intermittent Duty
- Maximum Force: 1.2 kg (41 oz)
- Maximum Stroke: 3/4"

2.2 Advantages / Disadvantages

The advantages of using this type of source are:

- Better control of the trigger and time zero
- More energy delivered

- Lower cost
- Easier handling of the rods, because there is no pressure pipe
- More control over the stacking procedure

The disadvantages are:

- More sensitive to water leakage inside the probe
- For deep soundings there is an increased probability of cross-talking between the trigger and the acquisition system
- The directivity function of the source is not obvious due to the upwards strike of the piston, and has yet to be determined

An example of the signals produced by this probe can be found in Appendix A

APPENDIX A

SAMPLE DATA PRODUCED BY SOURCE II

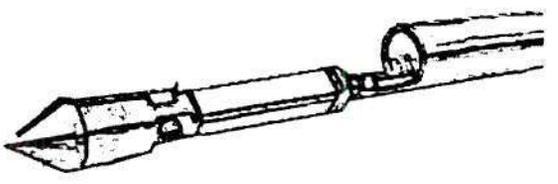

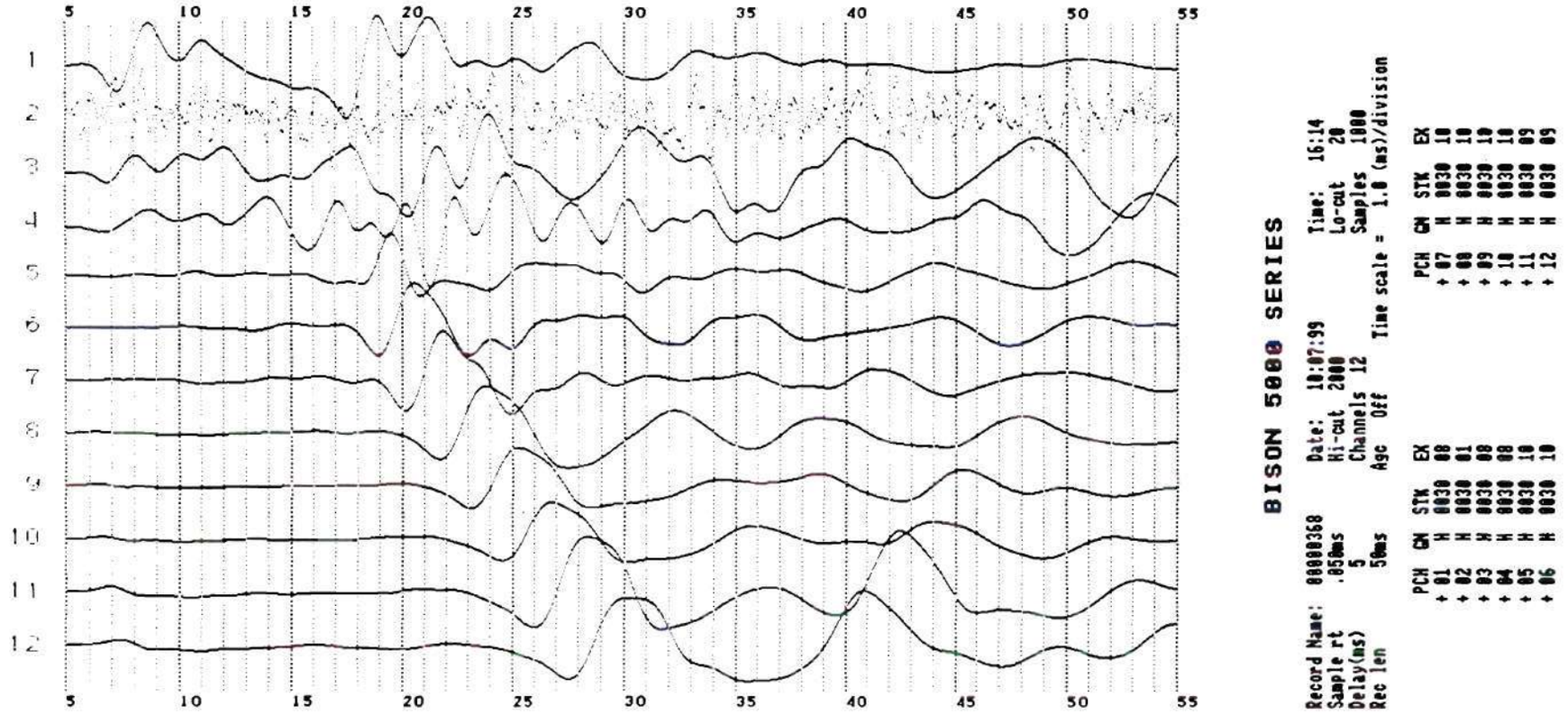

Sample Data 1. Borehole Separation: 4.6m. Depth: 2.5m

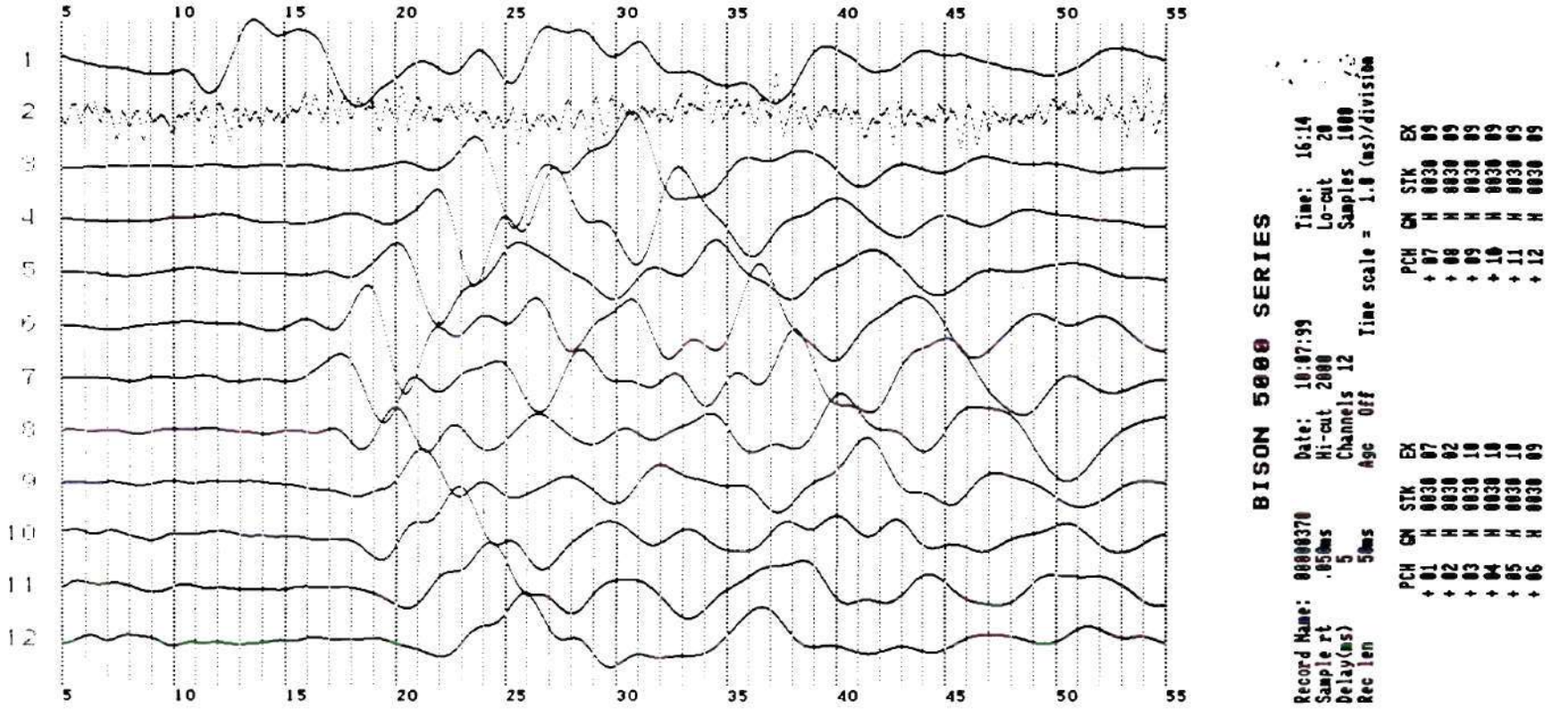

Sample Data 2. Borehole Separation: 4.6m. Depth: 4.3m

APPENDIX B
SOURCE SCHEMATICS

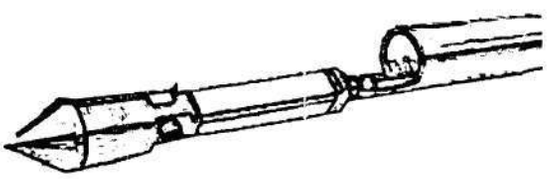

Particulate Media Lab

Title: Pneumatic Source Prototype I

(All measurements are in inches)

Date: Dec/15/98

Author: ALF

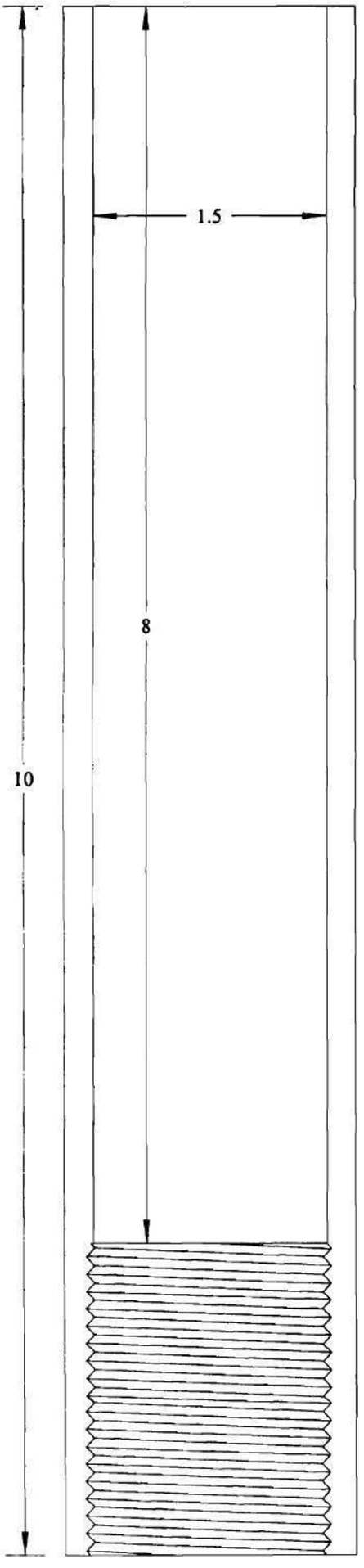

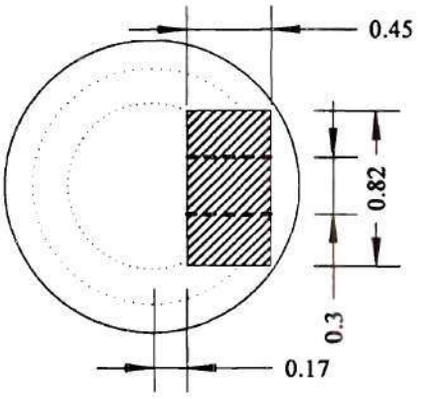

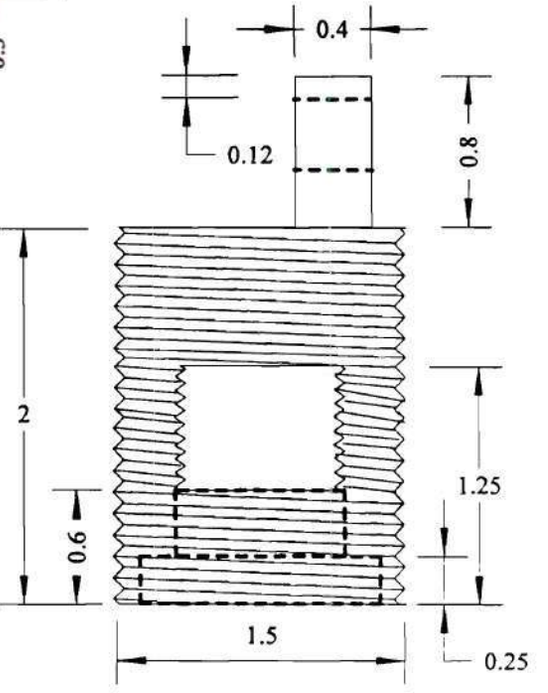

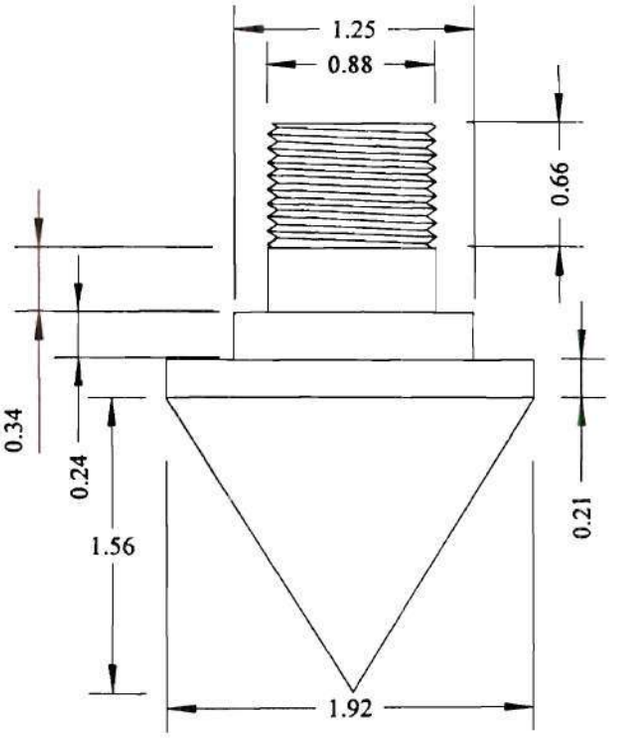

Particulate Media Lab

Title: Electric Source Prototype II

(All measurements are in inches)

Date: Jul/26/98

Author: ALF

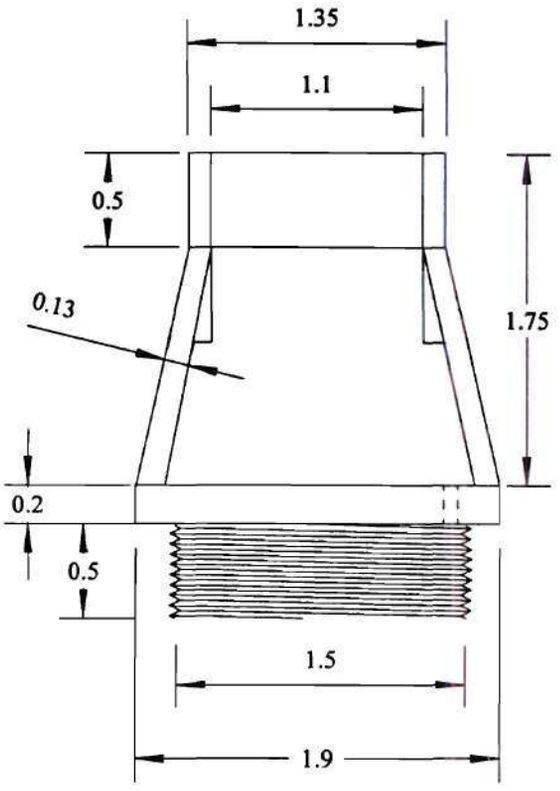

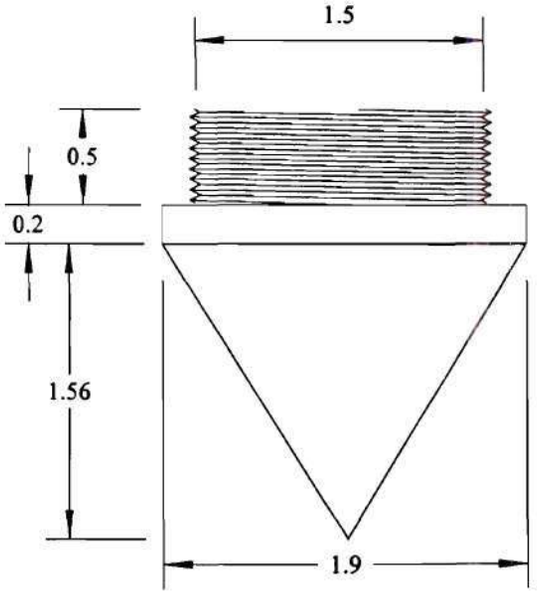

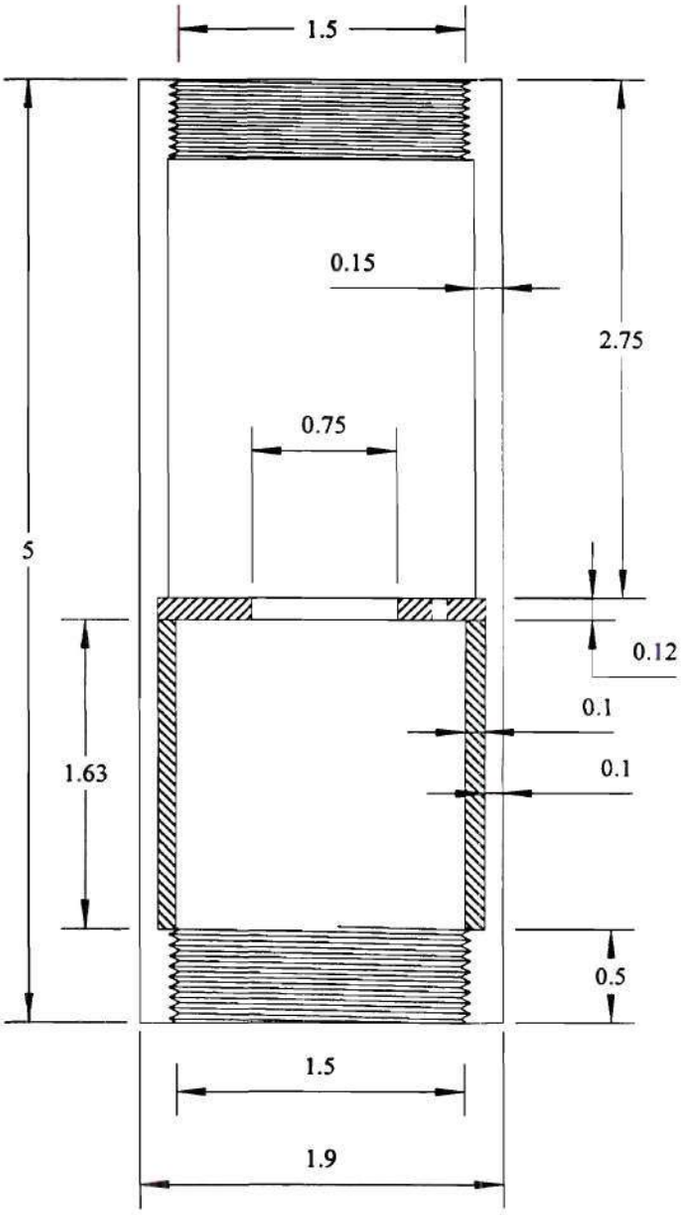

APPENDIX C
TECHNICAL SPECIFICATIONS

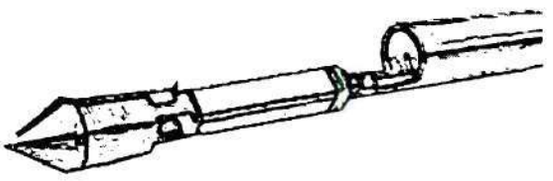

SPRINGLESS DOUBLE-IMPACT MATCH-PLATE VIBRATOR

The LA eliminates maintenance worries and down time that results from vibrator spring breakage. LA vibrator design incorporates an end intake connection with built-in swivel action, and patented features provide trouble-free operation. This vibrator is engineered to give long, uninterrupted service with lower operating costs. The LA is furnished with "el" type 3/8" (1.0 cm) hose fitting.

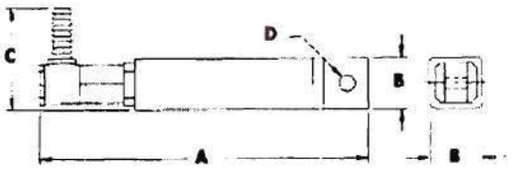

LA

PISTON DIA. in/cm	A in/cm	B in/cm	C in/cm	D in/cm	AIR CNSMP.* scfm/lpm (lpm=liters per min.) @60 psig 4.1 bar	FREQUENCY* (vibrations per min.) @60 psig 4.1 bar	WT. lbs/kg
5/8 1.6	6-9/16 16.7	1 2.5	2-1/4 5.7	3/8 1.0	3.8 108	14,100	1.5 0.7
3/4 1.9	6-5/8 16.8	1-3/16 3.0	2-3/8 6.0	3/8 1.0	5.4 153	13,600	2 0.9
1 2.5	6-15/16 17.6	1-1/2 3.8	2-1/2 6.4	1/2 1.3	5.8 164	11,700	3 1.4

*Frequency data obtained through testing under a no-load condition. Frequency will decline as load is increased.

Solenoids & Three-Phase Power Monitors

About Solenoids

Solenoids are electromechanical devices that exert force in a linear push or pull motion. *Stroke* is the distance the plunger travels. *Force* is the maximum energy exerted by the plunger. *Duty cycle* is the percentage of time that the solenoid can be energized. There are two duty cycle options. *Intermittent Duty*—Solenoid can be energized up to 25% of the time with a maximum "on" time of 100 seconds. *Continuous Duty*—Solenoid can be energized 100% of the time.

Box Frame Solenoids

Box frame solenoids have mounting holes on two sides to make installation easy. Put them to work actuating small on/off valves and electric door locks. Solenoids have Class A insulation and 0.187" quick-connect wiring lugs. UL recognized.

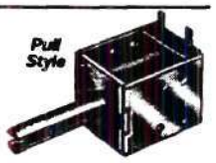

Coil Voltage	Max. Stroke	Force, oz.*	Coil Res., Ohms	Overall Size Lg.	Wd.	Ht.		Each
Pull Style								
Intermittent Duty								
12 DC	½"	25	12	1.1"	0.9"	1.2"	70155K56	$7.61
12 DC	¾"	45	8	1.8"	0.9"	1.2"	70155K49	9.65
12 DC	1"	100	4	2.0"	1.6"	1.6"	70155K43	12.39
24 DC	¾"	45	29	1.8"	0.9"	1.2"	70155K52	9.65
24 DC	1"	100	16	2.0"	1.6"	1.6"	70155K45	12.39
120 AC	¾"	25	85	1.8"	0.9"	1.2"	70155K47	9.96
120 AC	1"	36	37	2.0"	1.6"	1.6"	70155K41	14.76
Continuous Duty								
12 DC	½"	10	30	1.1"	0.9"	1.2"	70155K57	7.61
12 DC	¾"	22	18	1.8"	0.9"	1.2"	70155K51	9.65
12 DC	1"	60	16	2.0"	1.6"	1.6"	70155K44	12.39
24 DC	½"	10	116	1.1"	0.9"	1.2"	70155K59	7.61
24 DC	1"	60	61	2.0"	1.6"	1.6"	70155K46	12.39
120 AC	½"	11	410	1.1"	0.9"	1.2"	70155K55	8.53
120 AC	¾"	13	225	1.8"	0.9"	1.2"	70155K48	9.96
120 AC	1"	10	133	2.0"	1.6"	1.6"	70155K42	14.76
Push Style								
Intermittent Duty								
12 DC	¾"	41	8	1.8"	0.9"	1.2"	70155K63	13.12
120 AC	½"	16	220	1.1"	0.9"	1.2"	70155K65	15.16
120 AC	¾"	22	85	1.8"	0.9"	1.2"	70155K61	15.75
Continuous Duty								
12 DC	¾"	17	18	1.8"	0.9"	1.2"	70155K64	13.12
120 AC	½"	10	410	1.1"	0.9"	1.2"	70155K66	15.16
120 AC	¾"	11	225	1.8"	0.9"	1.2"	70155K62	15.75

★ At ⅛" stroke.

Laminated Solenoids

Laminated solenoids have a higher force rating than similar size box frame or tubular solenoids. The smaller-sized solenoids (1.6" × 1.2" × 1.4") have 0.187" quick-connect wiring lugs; larger-sized models (2.5" × 1.8" × 2.1") have solder lugs. All have Class A insulation. UL recognized.

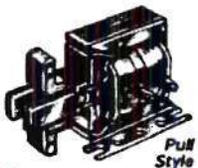

Coil Voltage	Max. Stroke	Force, oz.*	Coil Res., Ohms	Overall Size Lg.	Wd.	Ht.		Each
Pull Style								
Intermittent Duty								
120 AC	¾"	110	41	1.6"	1.2"	1.4"	7723K1	$21.37
120 AC	⅞"	190	8.8	2.5"	1.8"	2.1"	7723K5	26.31
240 AC	⅞"	190	45	2.5"	1.8"	2.1"	7723K7	26.31
Continuous Duty								
120 AC	¾"	63	85	1.6"	1.2"	1.4"	7723K2	21.37
120 AC	⅞"	90	20	2.5"	1.8"	2.1"	7723K6	26.31
240 AC	⅞"	90	78	2.5"	1.8"	2.1"	7723K8	26.31
Push Style								
Intermittent Duty								
120 AC	¾"	88	41	1.6"	1.2"	1.4"	7723K9	27.86
120 AC	⅞"	171	8.8	2.5"	1.8"	2.1"	7723K12	34.06
Continuous Duty								
120 AC	¾"	51	85	1.6"	1.2"	1.4"	7723K11	27.86
120 AC	⅞"	81	20	2.5"	1.8"	2.1"	7723K13	34.06

★ At ⅛" stroke.

Tubular Solenoids

Tubular design gives you the greatest force in a limited mounting space. Solenoids are completely enclosed in metal and resistant to vibration. Mounting hardware is included. For DC applications. UL recognized.

Coil Voltage	Max. Stroke	Force, oz.*	Coil Res., Ohms	Overall Size Dia.	Lg.		Each
Pull Style							
Intermittent Duty							
12 DC	¾"	15	12	0.75"	1.5"	69905K21	$10.53
12 DC	⅞"	41	9	1.00"	2.0"	69905K25	12.63
24 DC	⅞"	41	36	1.00"	2.0"	69905K27	12.63
Continuous Duty							
12 DC	¾"	8	31	0.75"	1.5"	69905K22	10.53
12 DC	⅞"	18	28	1.00"	2.0"	69905K26	12.63
24 DC	¾"	8	121	0.75"	1.5"	69905K24	10.53
24 DC	⅞"	18	110	1.00"	2.0"	69905K28	12.63
Push Style							
Intermittent Duty							
12 DC	⅞"	38	9	1.00"	2.0"	69905K35	14.94
24 DC	⅞"	38	36	1.00"	2.0"	69905K37	14.94
24 DC	1"	83	28	1.50"	1.6"	69905K31	20.02
24 DC	1"	100	22	1.50"	2.4"	69905K33	23.31
Continuous Duty							
12 DC	⅞"	15	28	1.00"	2.0"	69905K36	14.94
24 DC	⅞"	15	110	1.00"	2.0"	69905K38	14.94
24 DC	1"	30	90	1.50"	1.6"	69905K32	20.02
24 DC	1"	40	68	1.50"	2.4"	69905K34	23.31

★ At ⅛" stroke.

High-Force Laminated Solenoids

The highest rated force over the longest stroke length of any solenoid we offer. These solenoids are pull style, rated for continuous duty of up to 30 cycles per minute. The floating pole piece ensures accurate plunger pole alignment, keeps coil heating to a minimum, and reduces power loss and noise levels. Coil is varnish-impregnated to resist vibration, moisture, and shock. Solenoids have Class F insulation and include a cover.

Coil Voltage	Max. Stroke	Force, lbs.•	Coil Res., Ohms	Overall Size Lg.	Wd.	Ht.		Each
120 AC	1¼"	3	10.5	3.5"	2.6"	2.4"	6501K133	$192.86
120 AC	1¼"	5	5.2	3.5"	2.6"	2.6"	6501K143	271.43
120 AC	1½"	7	2.2	4.5"	3.7"	3.0"	6501K152	297.14
120 AC	1½"	10	1.8	4.5"	3.7"	3.3"	6501K162	305.71
120 AC	1½"	16	.92	4.5"	3.7"	3.7"	6501K171	334.33
120 AC	2½"	18	.35	6.0"	4.8"	4.1"	6501K183	434.33
120 AC	3½"	35	.12	7.9"	6.1"	4.9"	6501K213	785.71
230 AC	1¼"	3	42.0	3.5"	2.6"	2.4"	6501K134	192.86
230 AC	1¼"	5	27.0	3.5"	2.6"	2.6"	6501K144	271.43
230 AC	1½"	16	3.8	4.5"	3.7"	3.7"	6501K174	334.33
460 AC	1¼"	5	111.0	3.5"	2.6"	2.6"	6501K145	271.43
460 AC	1½"	7	34.6	4.5"	3.7"	3.0"	6501K155	297.14
460 AC	1½"	16	14.1	4.5"	3.7"	3.7"	6501K175	334.33
460 AC	2½"	25	5.0	6.0"	4.8"	4.8"	6501K195	478.46
460 AC	3½"	35	2.3	7.9"	6.1"	4.9"	6501K215	785.71

• At maximum stroke.

Three-Phase Power Monitors

Continuously monitor three-phase lines and motors for phase loss, low voltage, phase reversal, and phase unbalance using these solid state plug-in units. Applying correct voltage and phase rotation energizes the monitor's relay. A fault condition causes the relay to de-energize. They automatically reset when problem is corrected. A failure indicator makes adjustment and system troubleshooting easier. Monitors operate on 60 Hz and can be used on both "Y" and delta systems. Relays are single-pole, double-throw (SPDT), rated 10 amps at 240 VAC. All are UL recognized.

8-pin monitors are 3.25" Ht. × 1.95" Wd. × 1.95" Dp. 8-pin socket (sold separately) has screw terminals.

Panel-mount monitors are 6.06" Ht. × 3.88" Wd. × 2.08" Dp. They can be mounted on a 35 mm DIN rail using the adapter (sold separately).

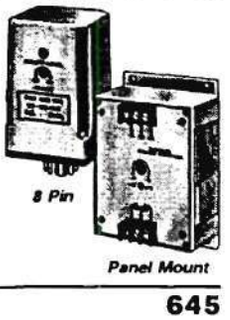

Max. Input, VAC	Adjust. Range, VAC	8 Pin	Each	Panel Mount	Each
120	85-120	6973K71	$77.19	6969K41	$127.19
240	160-240	6973K72	77.19	6969K42	127.19
480	380-480	6973K73	77.19	6969K43	127.19
575	450-575	———	———	6969K44	127.19
Accessories					Each
Socket for 8 Pin				7170K17	$4.20
DIN Rail Adapter for Panel Mount				6969K89	32.03

E-20-F09

Georgia Institute of Technology
School of Civil and Environmental Engineering
Geosystems department

DEVICE FOR SHEAR-WAVE MEASUREMENTS IN SOFT SEDIMENTS - PROTOTYPE -

Contents

October, 1999

DEVICE - SCHEMATIC

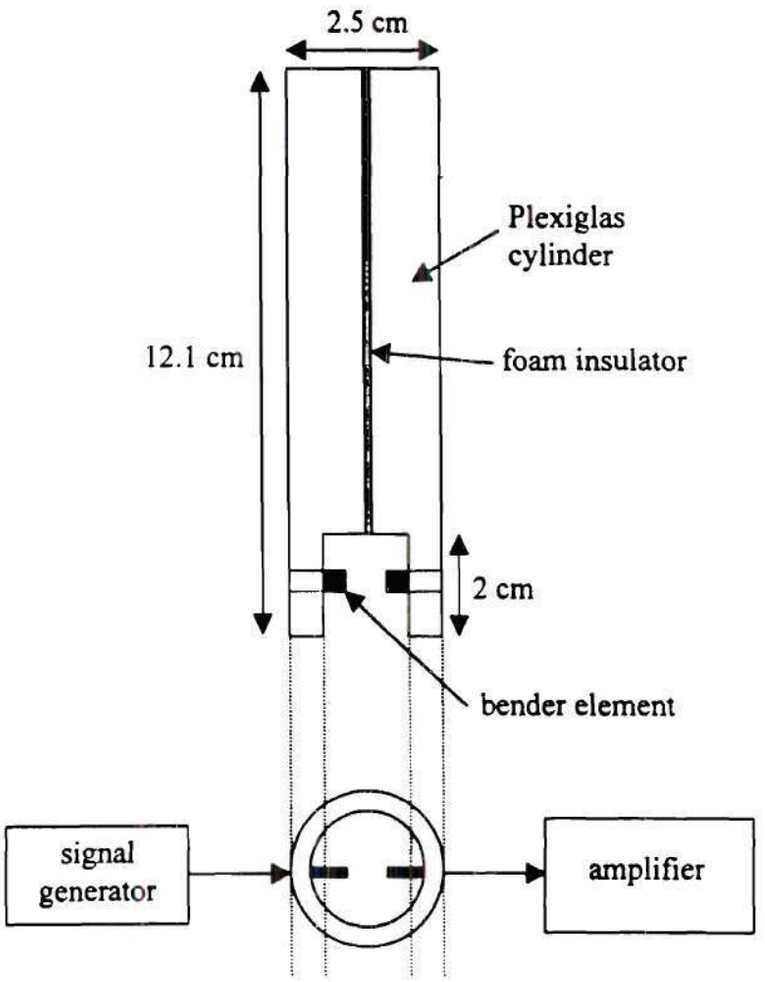

NOISE REDUCTION USING STACKING

Signal stacking is a very effective procedure to reduce the noise level of random noise in the signal. Random noise tends to cancel in the stacked signal.

Signal with a single measurement:

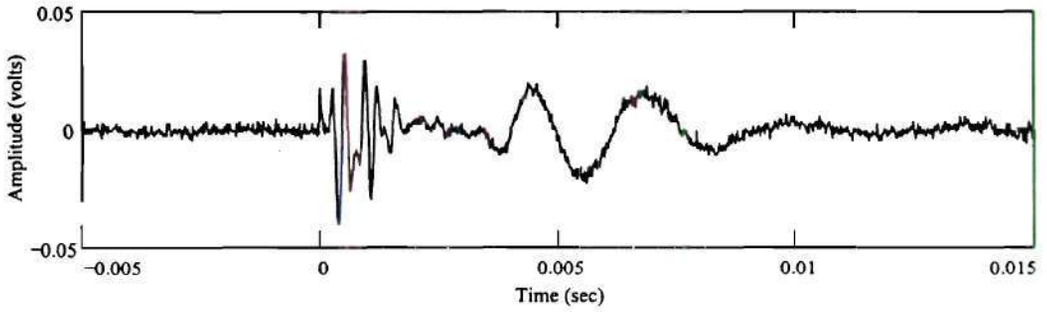

Signal after 100 stacks:

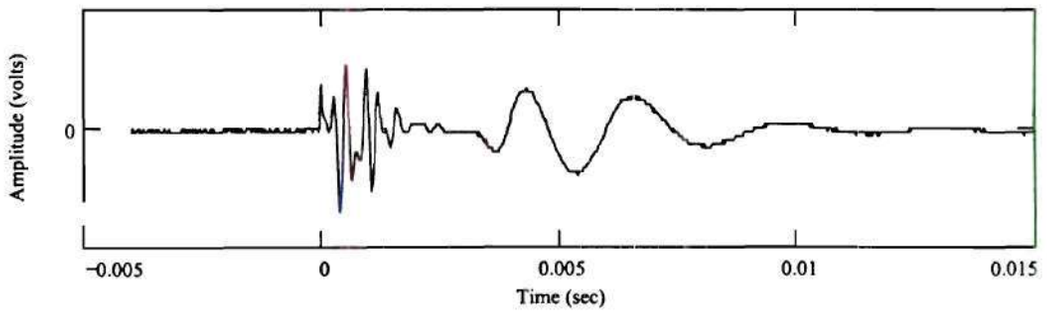

CROSS-TALK REDUCTION

Due to small separation of bender elements, small, there is a significant amount of cross-talk interfering with the signal. To reduce/avoid this effect, (1) coat with FR filter paint and (2) ground with metal electrodes should be place beside each bender element and they should be grounded together with the source's ground.

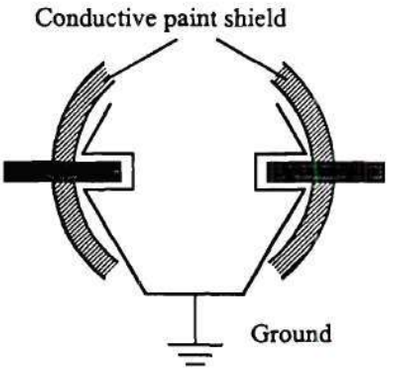

Non-Grounded Bender Elements:

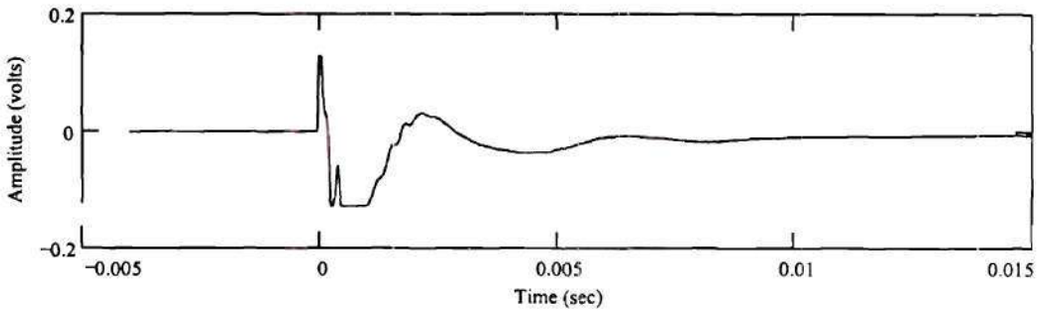

Grounded Bender Elements:

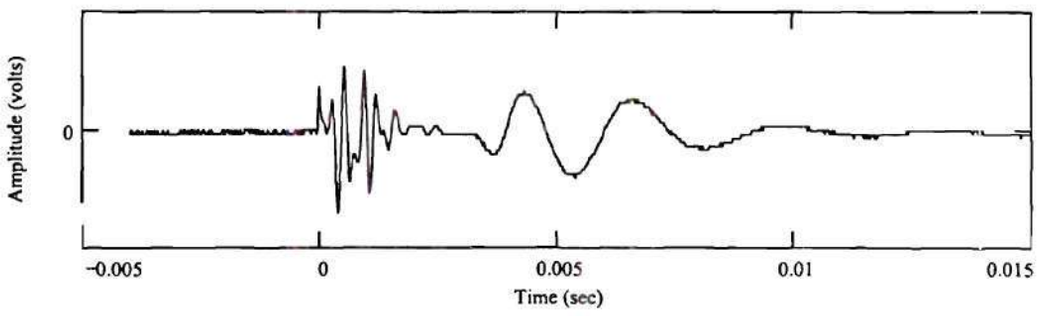

REDUCTION OF THE P-WAVE REFLECTIONS

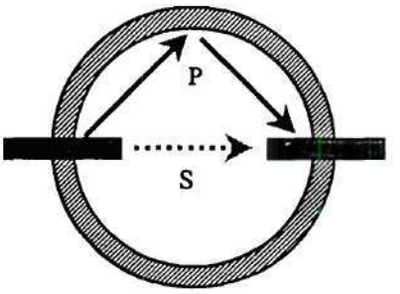

P-wave reflections from the walls of the probe can interfere with the arrival of the S-wave. Lateral "windows" are cut along the probe to avoid such reflections.

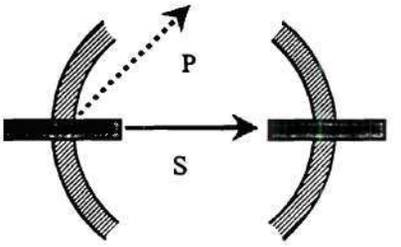

Probe without Lateral Windows:

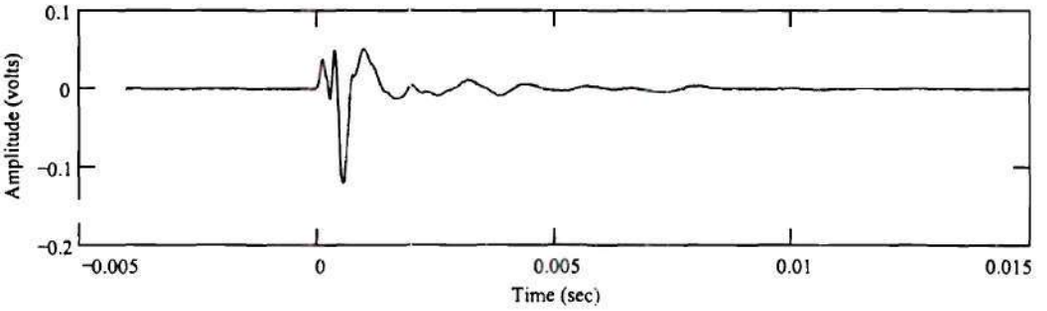

Probe with Lateral Windows:

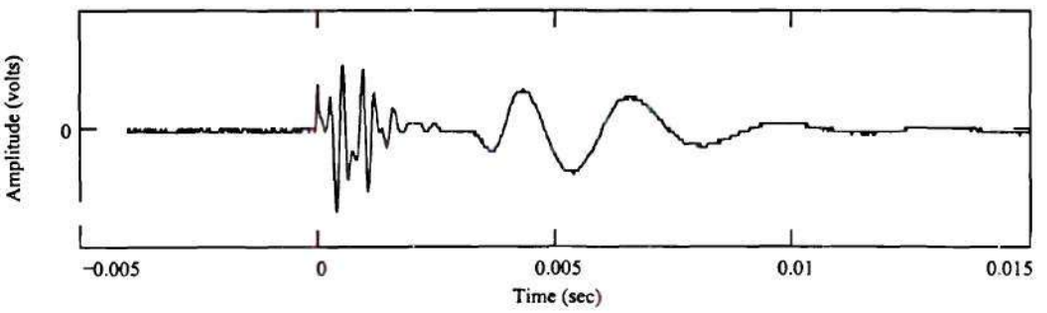

REDUCTION OF THE P-WAVE TRANSMITED

Body waves traveling through the shell of the probe add noise. The transmission of the body waves is avoided by splitting the probe in two, and keeping both halves without direct contact.

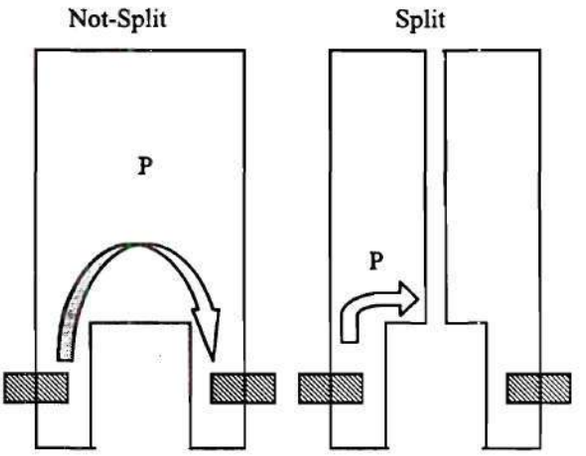

Not-split Probe:

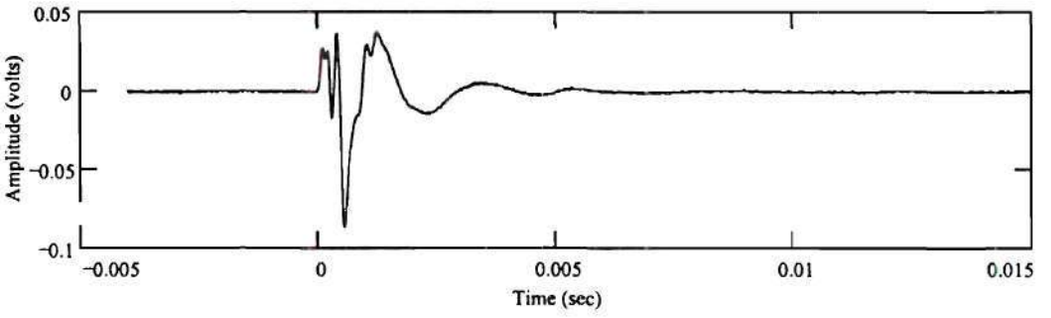

Probe with Isolated Bender Elements (Split Probe):

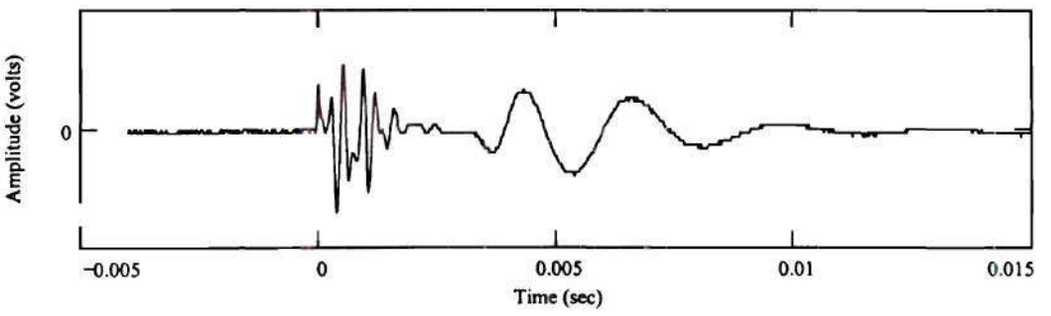

SIGNAL POST-PROCESSING

A low-pass filter can be applied to the signal to remove the high frequency noise.

FFT of the signal

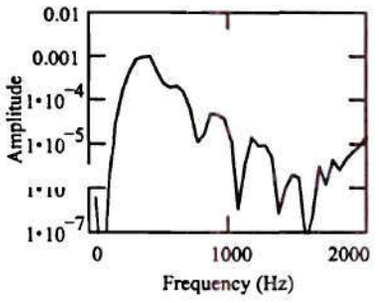

Low-Pass Filter

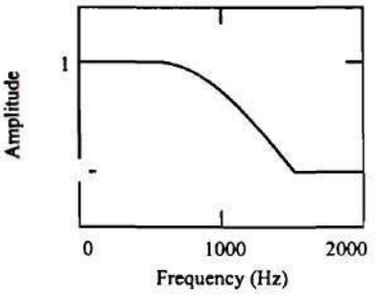

Raw Signal

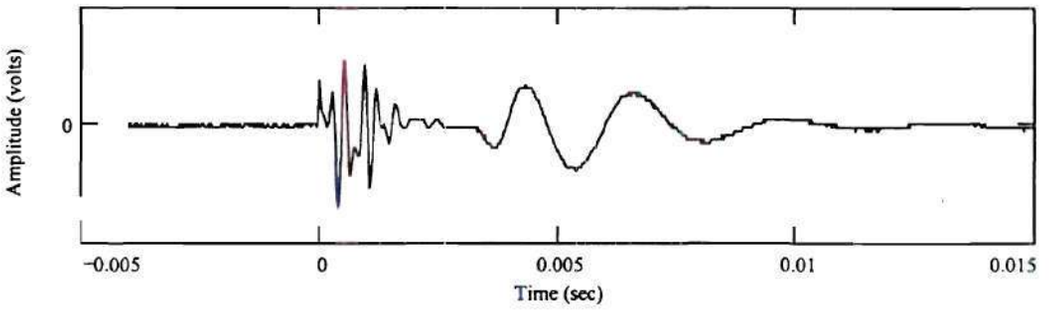

Filtered Signal

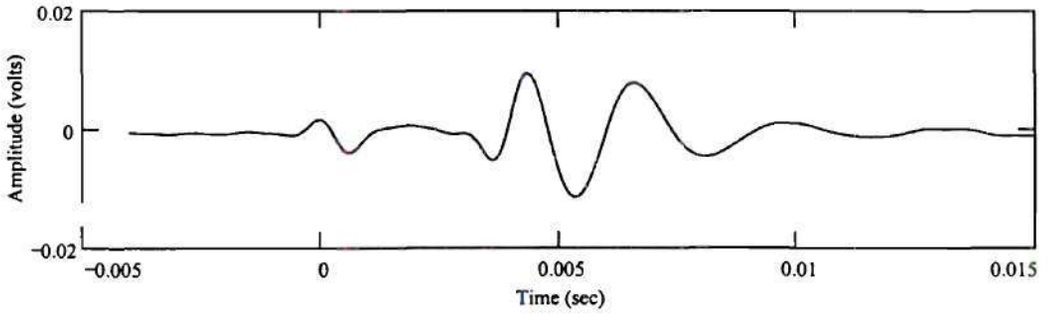

EXAMPLE: EVOLUTION OF CONSOLIDATION

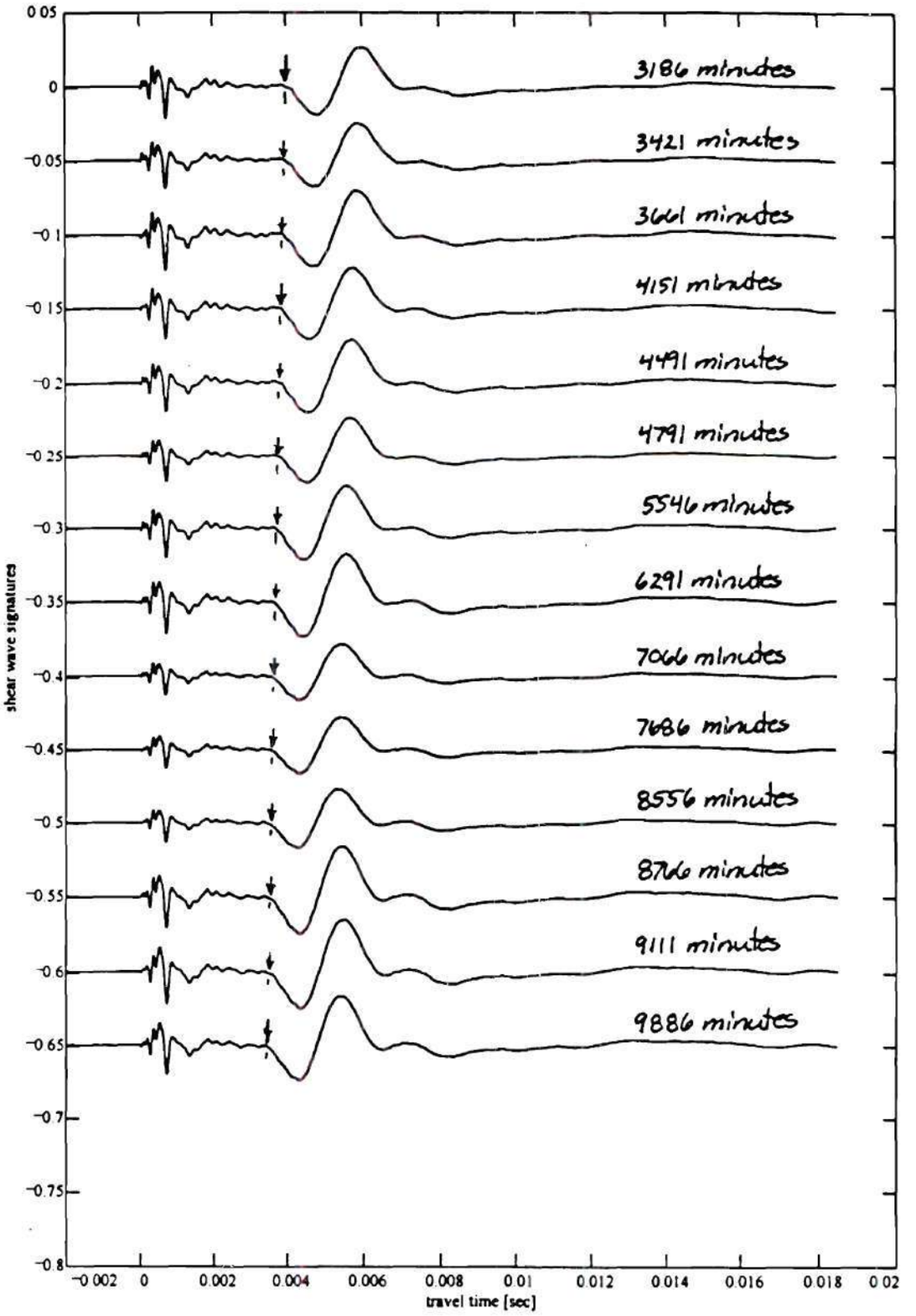

EXAMPLE OF APPLICATION

Shear Wave Velocity Profile from Providence River